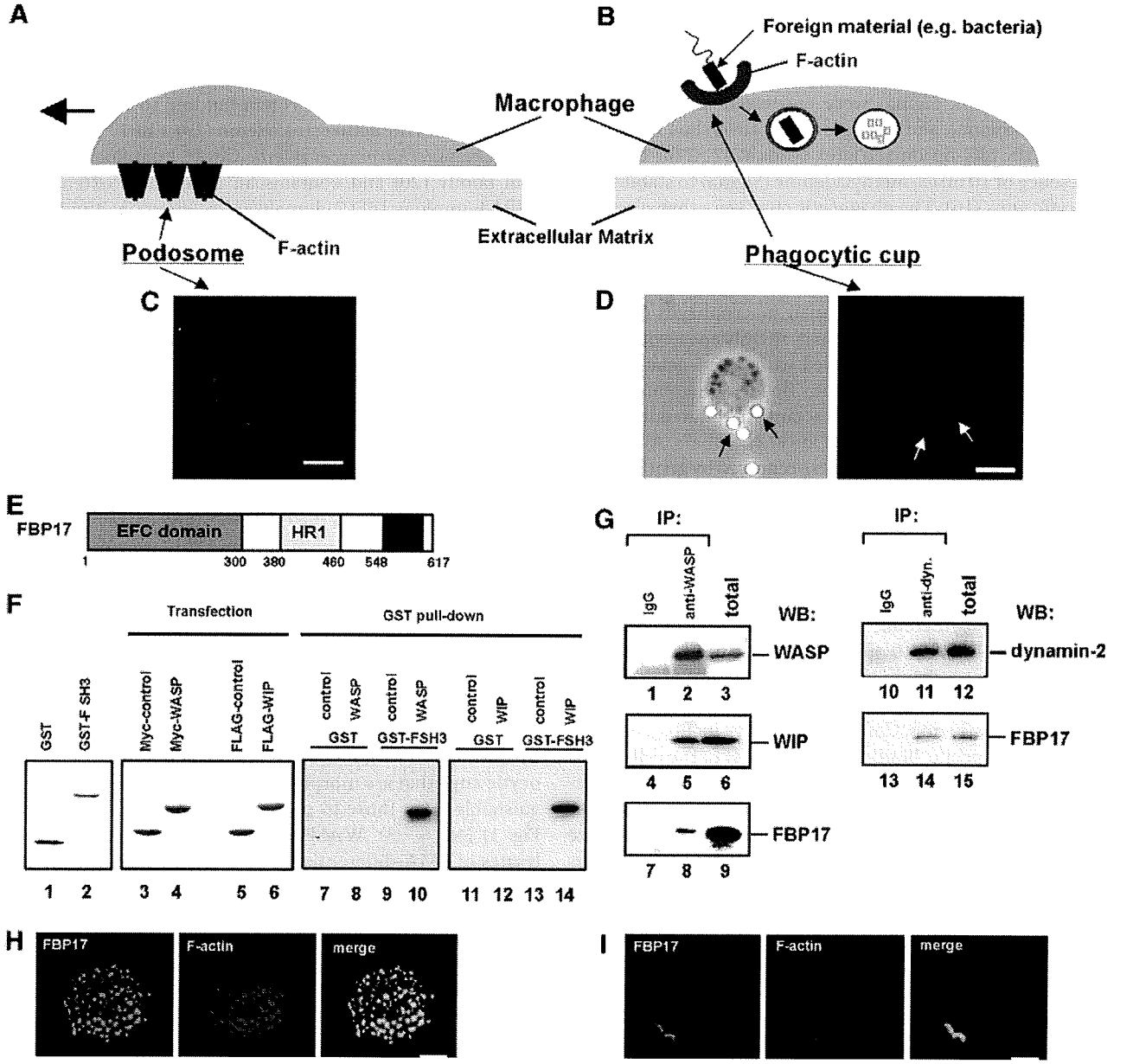

FIGURE 1. **FBP17 is a component of podosomes and phagocytic cups.** *A* and *B*, schematic drawings of podosomes (*A*) and a phagocytic cup (*B*) in macrophages. *C*, podosomes in macrophages were visualized by F-actin staining using Alexa Fluor 568-phalloidin. *D*, macrophages incubated with IgG-opsonized latex beads formed phagocytic cups to ingest the beads. A phase contrast image of a macrophage forming phagocytic cups (*left panel*). *Black arrows* indicate the latex beads ingested by the macrophage. Phagocytic cups were visualized by F-actin staining using Alexa Fluor 568-phalloidin (*right panel*). *White arrows* indicate the phagocytic cups. The *bar* is 10 μm. *E*, the domain organization of FBP17. *HR1*, protein kinase C-related kinase homology region 1. *F*, FBP17 interacts directly with WASP and WIP via its SH3 domain. GST and the GST-FBP17 SH3 domain fusion protein (GST-FSH3) were purified from bacteria extracts. Purified proteins were subjected to SDS-PAGE and stained with Coomassie Brilliant Blue (*lanes 1* and *2*). HEK293 cells were transfected with the cDNAs of Myc-tagged control protein (Myc-PDZ-GEF), Myc-WASP, FLAG-PDZ-GEF, or FLAG-WIP, and the expression of those proteins were analyzed by immunoblotting (*lanes 3–6*). Lysates from the HEK293 transfected cells were incubated with the affinity matrices of GST alone or GST-FSH3. Pull-down samples were analyzed by immunoblotting using anti-Myc antibody (*lanes 7–10*) and anti-FLAG antibody (*lanes 11–14*). *G*, FBP17 binds WASP, WIP, and dynamin-2. WASP was immunoprecipitated (*IP*) from the lysates of PMA-differentiated THP-1 cells with anti-WASP or a control IgG (*left panel, lanes 1–9*). The WASP immunoprecipitates and total lysates were analyzed by immunoblotting (*WB*) for WASP (*lanes 1–3*), WIP (*lanes 4–6*), and FBP17 (*lanes 7–9*). Dynamin was also immunoprecipitated from the THP-1 cell lysates with an anti-dynamin polyclonal antibody. The dynamin immunoprecipitates and total lysates were analyzed by immunoblotting for dynamin-2 (*lanes 10–12*) and FBP17 (*lanes 13–15*). *H* and *I*, confocal laser scanning micrographs of PMA-differentiated THP-1 cells. *H*, THP-1 cells transfected with FLAG-tagged FBP17 cDNA (FBP17) were double-stained with an anti-FLAG monoclonal antibody (*left panel*) and phalloidin (*center panel*) to visualize the F-actin in podosomes. *Yellow* indicates co-localization of FBP17 (*green*) and F-actin, podosomes (*red*) (*right panel*). *I*, THP-1 cells transfected with FLAG-FBP17 cDNA were incubated with IgG-opsonized latex beads and double-stained with anti-FLAG antibody and phalloidin. Phagocytic cups were visualized by F-actin staining (*center panel*). *Yellow* indicates co-localization of FBP17 (*green*) and F-actin, phagocytic cups (*red*) (*right panel*). The *bar* is 10 μm.

siRNAs-transfected cells, and analyzed the expression level of FBP17 by immunoblotting. THP-1 cells transfected with the siRNA for FBP17 expressed ~40% less FBP17 than cells transfected with a scrambled control siRNA based on the immunoblots (Fig. 2*A*, *lanes 1* and *2*) but expressed the same level of β-actin (Fig. 2*A*, *lanes 3* and *4*). The transfection efficiency of

Role of FBP17 in the Podosome and Phagocytic Cup Formation

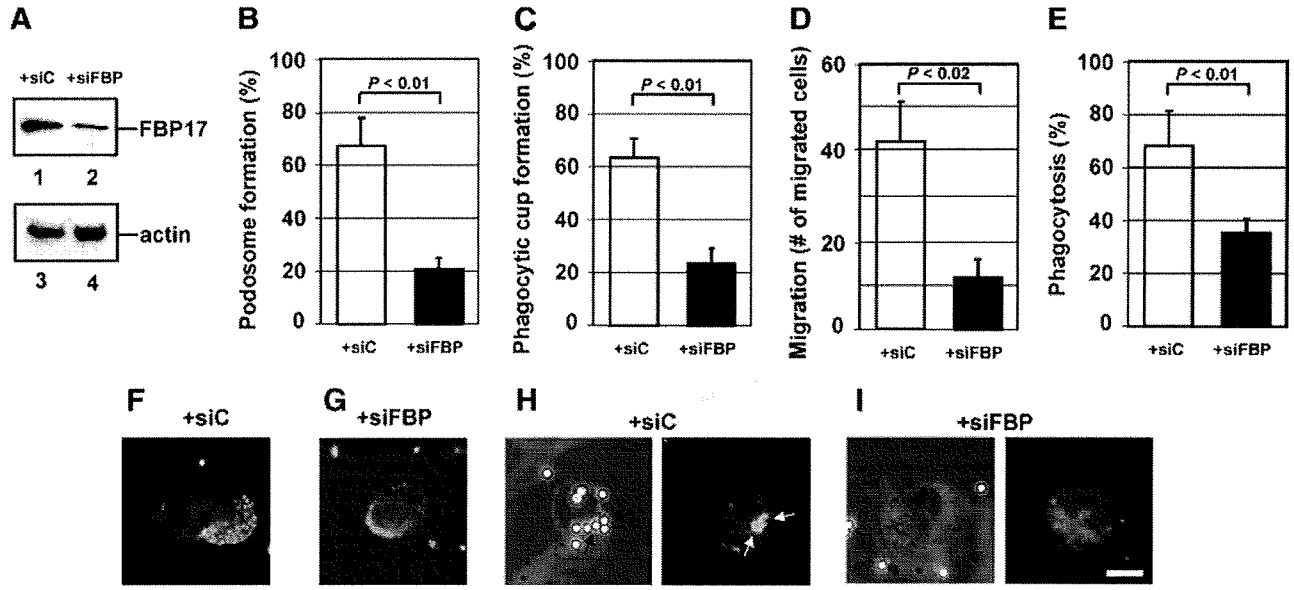

FIGURE 2. **The importance of FBP17 in the formation of podosomes and phagocytic cups.** *A*, expression of FBP17 was reduced by transfection of siRNA. THP-1 cells were transfected with siRNA for FBP17 (siFBP; *lanes 2* and *4*) or its scrambled control siRNA (siC; *lanes 1* and *3*). Lysates prepared from total transfected cells were analyzed by immunoblotting for FBP17 (*lanes 1* and *2*) and β-actin (*lanes 3* and *4*). *B* and *C*, effects of FBP17 siRNA on the formation of podosomes and phagocytic cups in macrophages. Human primary monocytes were co-transfected with siFBP (*closed bars*) or siC (*open bars*) and an FITC-conjugated control siRNA and then differentiated into macrophages with M-CSF-1. FITC-positive transfected cells were examined for the formation of podosomes (*B*) or phagocytic cups (*C*), and the percentage of cells with podosomes or phagocytic cups was scored. *D* and *E*, effects of FBP17 siRNA on the functions of podosomes and phagocytic cups. Macrophages co-transfected with siFBP (*closed bars*) or siC (*open bars*) and the FITC-conjugated control siRNA were assayed for macrophage migration (*D*) or phagocytosis of IgG-opsonized latex beads (*E*). Data represent the mean ± S.D. of triplicate experiments. *F–I*, immunofluorescence micrographs of a representative cell from each experiment. Cells transfected with siC (*F*) and siFBP (*G*) were stained with Alexa Fluor 568-phalloidin. Cells transfected with siC (*H*) or siFBP (*I*) were incubated with IgG-opsonized latex beads and then stained with phalloidin. The *left* and *right panels* are phase contrast and immunofluorescence micrographs, respectively. The *bar* is 10 μm.

THP-1 cells was estimated to be 40–50% from the expression of green fluorescent protein (GFP) used as a transfection control. Therefore, the decrease in FBP17 expression indicates that FBP17 was efficiently knocked down in most transfected cells.

Human primary monocytes were co-transfected with the FBP17 siRNAs and a FITC-conjugated control siRNA as a transfection marker. After differentiation of the monocytes into macrophages with M-CSF-1, FITC-positive cells were examined for the formation of podosomes and phagocytic cups. To quantify their formation, we scored the percentage of cells with podosomes or phagocytic cups among FITC-positive cells. When the expression of FBP17 was knocked down, the formation of both podosomes and phagocytic cups in macrophages was significantly reduced ($p < 0.01$; Fig. 2, *B* and *C*). These results suggest that FBP17 is necessary for the formation of podosomes and phagocytic cups. A representative cell from each experiment is shown in Fig. 2, *F* and *G*, for podosomes and in Fig. 2, *H* and *I*, for phagocytic cups. We then assayed macrophage migration as a podosome function and phagocytosis as a phagocytic cup function. When expression of FBP17 was knocked down, macrophage migration through a gelatin filter toward a chemoattractant was significantly reduced in cells transfected with FBP17 siRNA ($p < 0.02$; Fig. 2*D*). Phagocytosis of IgG-opsonized latex beads was also reduced (Fig. 2*E*). These results suggest that FBP17 is essential for chemotaxis and phagocytosis because of its role in forming podosomes and phagocytic cups, respectively.

FBP17 Recruits the WASP-WIP Complex to the Plasma Membrane—Recent biochemical analyses revealed that FBP17 binds to a membrane phospholipid, phosphatidylinositol 4,5-bisphosphate ($PI(4,5)P_2$), through its EFC/F-BAR domain and to N-WASP and dynamin via its SH3 domain (18, 21, 24). We have shown that although WASP and WIP are cytosolic proteins, the WASP-WIP complex localizes at podosomes and phagocytic cups (4, 16). We then examined whether FBP17 recruits the WASP-WIP complex to the plasma membrane in macrophages. We focused on the roles of the EFC and SH3 domains of FBP17 and constructed three FBP17 mutants for the recruitment experiments: a Lys-33 to Glu (K33E) substitution, a Lys-166 to Ala (K166A) substitution, and an SH3 domain deletion (dSH3). Both substitution mutations in the EFC domain (K33E and K166A) significantly reduce membrane binding and deformation (22), and the dSH3 mutant does not bind to WASP and WIP because the SH3 domain is the binding site of WASP and WIP (Fig. 1*F*). We co-transfected HEK293 cells with the FLAG-tagged FBP17 constructs, WASP, and WIP. A C-terminal fragment (1146–1429 amino acids) of PDZ-GDP exchange factor (PDZ-GEF) was used as a negative control for FBP17 because this fragment is stable in the cytosol and does not interact with any WASP-related proteins (4, 16, 25). We confirmed the expression of FBP17 and its mutants in cells by immunoblotting (supplemental Fig. 2) and immunoprecipitated FLAG-tagged proteins from lysates of the transfected cells with anti-FLAG antibody (Fig. 3*A*, *lanes 1–5*). WASP and WIP were detected in the immunoprecipitates from cells

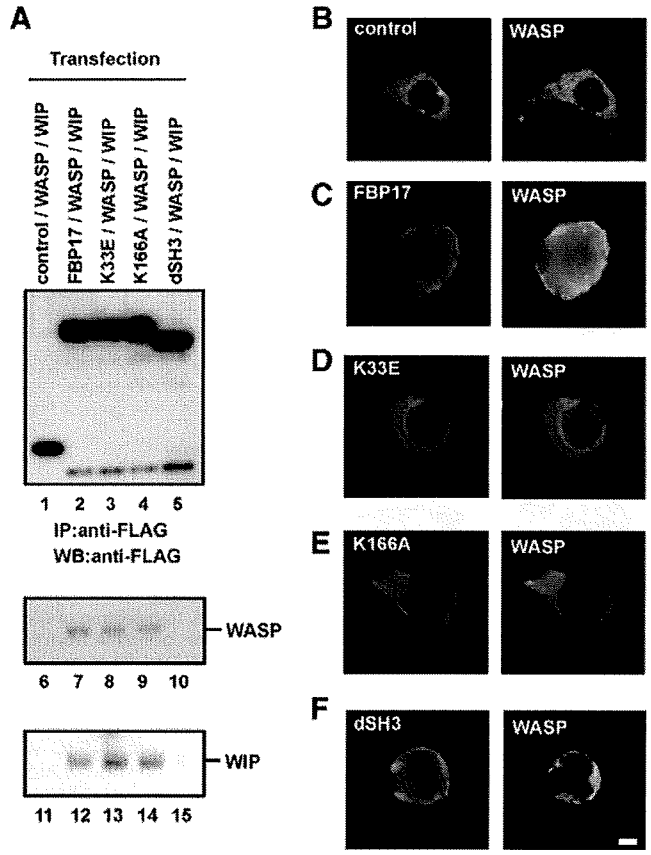

FIGURE 3. **FBP17 recruits WASP, WIP, and dynamin-2 to the plasma membrane.** *A*, HEK293 cells were co-transfected with cDNAs of the indicated FLAG-tagged proteins, Myc-tagged WASP, and HA-tagged WIP. The FLAG-tagged proteins were immunoprecipitated (*IP*) from lysates of the transfected cells with an anti-FLAG antibody followed by immunoblotting (*WB*) using antibodies to FLAG (*lanes 1–5*), WASP (*lanes 6–10*), and WIP (*lanes 11–15*). *B–F*, transfected HEK293 cells expressing FLAG-tagged proteins, Myc-WASP, and HA-WIP were double-stained with an anti-FLAG antibody and anti-WASP antibody. *B–F*, cells expressing FLAG-PDZ-GEF (*B*), FLAG-FBP17 (*C*), the FLAG-tagged FBP17 mutant with the K33E missense mutation (*D*), K166A (*E*), and the SH3-deleted FBP17 mutant dSH3 (*F*). The *bar* is 10 μm.

expressing the FLAG-tagged FBP17, K33E, and K166A constructs (Fig. 3*A*, *lanes 7–9* and *12–14*) but not the FLAG-tagged PDZ-GEF and dSH3 constructs (Fig. 3*A*, *lanes 6*, *10*, *11*, and *15*), indicating that FBP17 and its mutants K33E and K166A form a complex with WASP and WIP but that dSH3 not.

Next, cells expressing the FLAG-tagged proteins, WASP, and WIP were examined under the immunofluorescence microscope for the localization of the FLAG-tagged proteins and WASP. WASP and WIP were localized in the cytosol in cells transfected with only the WASP cDNA and only the WIP cDNA, respectively, as well as in cells expressing both WASP and WIP (supplemental Fig. 3). In cells co-expressing FLAG-PDZ-GEF (control) with WASP and WIP, both FLAG-PDZ-GEF and WASP were cytosolic (Fig. 3*B*). In cells co-expressing FLAG-FBP17 with WASP and WIP, FLAG-FBP17 localized at the plasma membrane because its EFC domain binds to the plasma membrane (Fig. 3*C*, *left panel*). In those cells, WASP also localized at the plasma membrane (Fig. 3*C*, *right panel*), indicating that FBP17 shifted the localization of WASP from the cytosol to the plasma membrane (Fig. 3, *B* and *C*). To confirm that the WASP-WIP complex was recruited to the plasma membrane, cells co-expressing FLAG-FBP17 with WASP and HA-tagged WIP were stained with an anti-FLAG monoclonal antibody and an anti-WASP polyclonal antibody or an anti-HA rat monoclonal antibody. Double staining revealed that both WASP and WIP co-localized with FLAG-FBP17 at the plasma membrane (supplemental Fig. 4, *A* and *B*). To further confirm the localization of the FBP17 mutants, cells co-expressing the FLAG-tagged FBP mutants, WASP, and WIP were stained with anti-FLAG monoclonal antibody. The K33E and K166A mutants were cytosolic and the SH3-deleted FBP17 mutant localized at the plasma membrane (supplemental Fig. 4*C*).

To determine the roles of the EFC and SH3 domains of FBP17 in this recruitment, we examined the localization of the FBP17 mutants and WASP in cells co-expressing the FBP mutants with WASP and WIP. Membrane tubulation in cells transfected with an FBP17 cDNA is an indicator of the membrane binding and deformation activities of FBP17 (18, 22). We detected *in vivo* membrane tubulation in cells expressing FBP17 and dSH3 but not in cells expressing K33E and K166A (supplemental Fig. 5). In cells co-expressing either FBP17 mutant (K33E or K166A) with WASP and WIP, both K33E and K166A were cytosolic (Fig. 3, *D* and *E*, *left panels*), and WASP was also cytosolic (Fig. 3, *D* and *E*, *right panels*). These results indicate that K33E and K166A are unable to recruit WASP to the plasma membrane, consistent with the inability of K33E and K166A to bind and deform the plasma membrane (supplemental Fig. 5).

The SH3-deleted FBP17 mutant, dSH3, localized at the plasma membrane (Fig. 3*F*, *left panel*) because its EFC domain is intact. However, WASP was cytosolic in cells co-expressing dSH3 with WASP and WIP (Fig. 3*F*, *right panel*), consistent with the inability of the dSH3 mutant to bind to WASP and WIP (Fig. 3*A*, *lanes 5*, *10*, and *15*).

To quantify the recruitment, we scored the percentage of cells in which WASP and WIP were localized at the plasma membrane. Cells expressing the FBP17 mutants (K33E, K166A, or dSH3) exhibited significantly lower plasma membrane localization of WASP and WIP than cells expressing FBP17 ($p < 0.05$; supplemental Fig. 6, *A* and *B*). FBP17 also recruited dynamin-2 to the plasma membrane, and both EFC and SH3 domains are necessary for this recruitment (supplemental Fig. 6*C*), as reported previously (18, 21). To confirm the localization of FBP17 and its mutants in cells co-expressing FBP17 with WASP, WIP, and dynamin-2, the transfected cells were stained with anti-FLAG monoclonal antibody. The wild-type FBP17 and dSH3 localized at the plasma membrane and the FLAG-PDZ-GEF (control) and the FBP mutants (K33E and K166A) were cytosolic (supplemental Fig. 6*D*).

Subcellular Localization of FBP17, WASP, WIP, and Dynamin-2 in Macrophages—To determine whether WASP, WIP, and dynamin-2 are recruited to the plasma membrane in macrophages when podosomes and phagocytic cups are formed, we examined the subcellular localization of FBP17, WASP, WIP, and dynamin-2 in macrophages forming podosomes or phagocytic cups. The cytosolic and membrane fractions were prepared from macrophages and analyzed by immunoblotting. Caspase-3 is a cytosolic marker, and sodium

potassium ATPase is a plasma membrane marker (26). FBP17 was detected in the membrane fraction from macrophages forming podosomes (Fig. 4*A*, *lane 9*). WASP, WIP, and dynamin-2 were also detected in the membrane fraction, although they are cytosolic proteins (Fig. 4*A*, *lanes 12*, *15*, and *18*). FBP17 was detected in the membrane fraction from macrophages forming phagocytic cups (Fig. 4*B*, *lane 9*). WASP, WIP, and dynamin-2 were also detected in the membrane fractions from macrophages forming phagocytic cups (Fig. 4*B*, *lanes 12*, *15*, and *18*). These results, taken together with Fig. 3, suggest that FBP17 recruits the WASP-WIP complex and dynamin-2 to the plasma membrane in macrophages and that both the EFC and the SH3 domains are necessary for this recruitment.

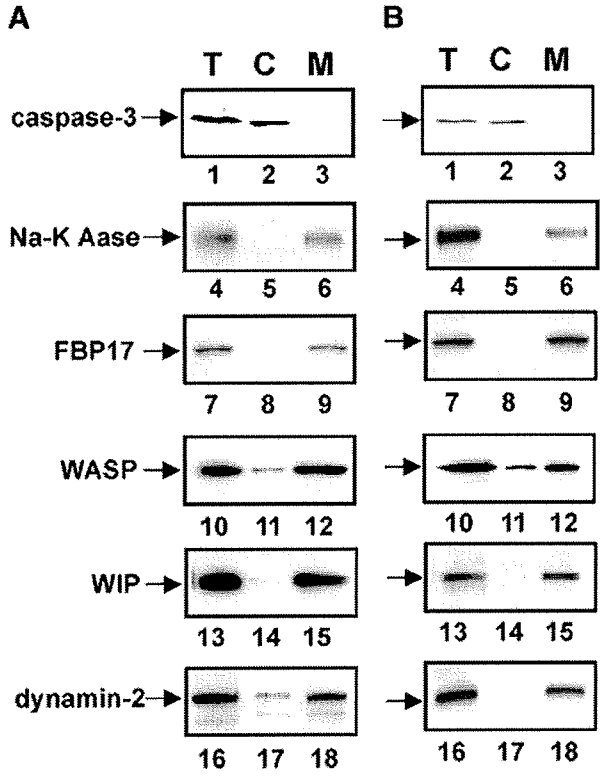

FIGURE 4. **Subcellular localization of FBP17, WASP, WIP, and dynamin-2 in macrophages.** *A*, macrophages forming podosomes. *B*, macrophages forming phagocytic cups. Total lysates (*T*), the cytosolic fraction (C), and the membrane fraction (*M*) prepared from macrophages forming podosomes (*A*) or phagocytic cups (*B*) were analyzed by immunoblotting for caspase-3 (*lanes 1–3*), sodium potassium ATPase (*Na-K Aase*; *lanes 4–6*), FBP17 (*lanes 7–9*), WASP (*lanes 10–12*), WIP (*lanes 13–15*), and dynamin-2 (*lanes 16–18*). Caspase-3 and sodium potassium ATPase (Na-K ATPase) are markers for the cytosol and plasma membrane, respectively.

The Role of Each Domain of FBP17 in the Formation of Podosomes and Phagocytic Cups—To determine the roles of the EFC and SH3 domains in the formation of podosomes and phagocytic cups, we examined whether overexpression of the FBP17 mutants affects the formation of these structures. We transfected THP-1 cells with the FBP17 constructs and confirmed the expression of FBP17 or the FBP17 mutants in transfected THP-1 cells by immunoblotting (Fig. 5*A*). When THP-1 cells were differentiated to obtain macrophage phenotypes with PMA, podosome formation was significantly reduced in cells overexpressing the K33E, K166A, and dSH3 FBP17 mutants when compared with the FBP17 wild type ($p < 0.01$; Fig. 5*B*). Phagocytic cup formation was also reduced in cells overexpressing the FBP17 mutants (Fig. 5*C*). These results indicate that the EFC domain and SH3 domain are essential for the formation of podosomes and phagocytic cups in macrophages.

Defects in Macrophages from WAS Patients—Our results suggest that the complex formation of FBP17 with WASP, WIP, and dynamin-2 at the plasma membrane is a critical step in the formation of podosomes and phagocytic cups (Figs. 1*G*, 3, and 4). In macrophages from WASP-deficient WAS patients, the complex does not form properly due to a lack of WASP expression. We examined macrophages from WASP-deficient WAS patients for the formation of podosomes and phagocytic cups. Two genetically independent WAS patients (WAS1, 211delT; and WAS2, 41–45delG) (27, 28) were assayed for the formation of those structures. Podosomes were completely absent (Fig. 6, *A–C*), and phagocytic cup formation was severely impaired (Fig. 6, *D–F*) in macrophages from both WAS patients, although FBP17, WIP, and dynamin-2 were expressed at the same level in patients as in normal individuals (Fig. 6*G*). In fact, the formation of podosomes and phagocytic cups was impaired in macrophages when the expression of WASP was reduced by siRNA transfection (4, 16). This is the first result showing that both podosome and phagocytic cup formations are defective in macrophages from WASP-deficient patients. These results are consistent with the previous observations (3, 12).

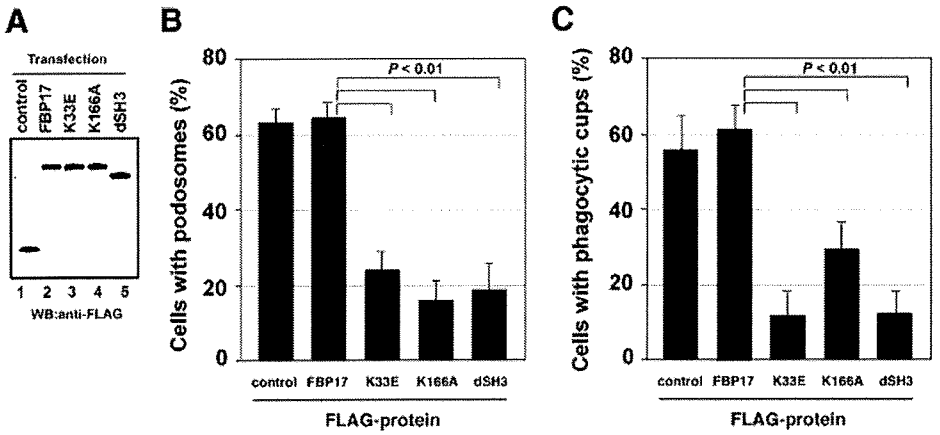

FIGURE 5. **The role of the EFC and SH3 domains of FBP17 in the formation of podosomes and phagocytic cups.** *A*, expression of FLAG-tagged proteins in transfected THP-1 cells. Total lysates prepared from transfected THP-1 cells were analyzed by immunoblotting (*WB*) using an anti-FLAG antibody. All of the FLAG-tagged proteins, FLAG-PDZ-GEF (control, *lane 1*), FLAG-FBP17 (*lane 2*), and the FBP17 mutants, K33E, K166A, and dSH3 (*lanes 3–5*) were expressed in THP-1 cells at similar levels. *B* and *C*, THP-1 cells co-transfected with cDNAs for the FLAG-tagged proteins and pmaxGFP were differentiated with PMA and then assayed for the formation of podosomes (*B*) and phagocytic cups (*C*). The percentage of cells with podosomes or phagocytic cups among all GFP-positive cells was scored. Data represent the mean ± S.D. of triplicate experiments.

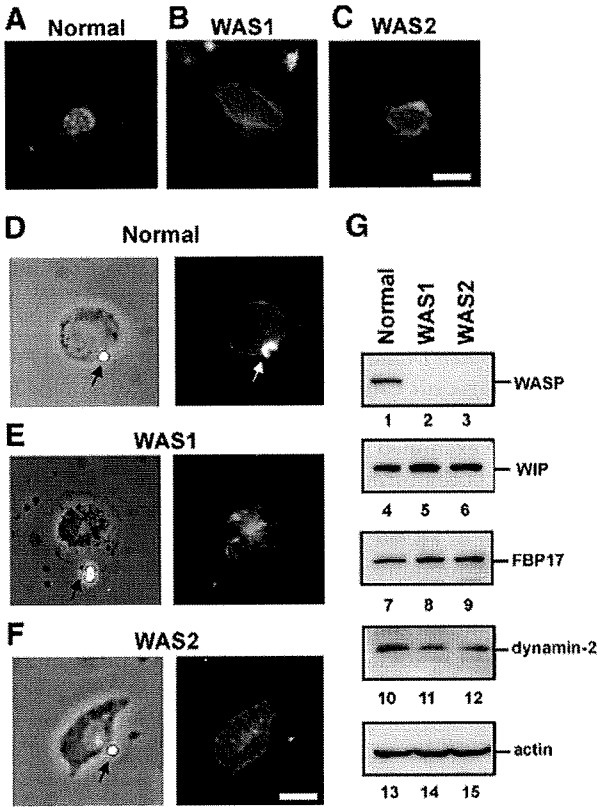

FIGURE 6. **Defective formation of podosomes and phagocytic cups in macrophages from WAS patients.** *A–F*, macrophages from a normal control and two genetically independent WAS patients (WAS1 and WAS2) were examined for the formation of podosomes (*A–C*) and phagocytic cups (*D–F*). The patients, WAS1 and WAS2, have the deletion mutations 211delT and 41–45delG, respectively, in their genomic DNAs. The *bars* are 10 μm. *G*, expression levels of WASP, WIP, FBP17, dynamin-2, and β-actin in WAS patients. Lysates prepared from macrophages from a normal control and two WAS patients (WAS1 and WAS2) were subjected to immunoblotting. WASP was not detected in the lysates from these WAS patients (*lanes 2* and *3*). Podosomes were completely absent (*A–C*) and phagocytic cup formation was severely impaired (*D–F*) in macrophages from both WAS patients, although FBP17, WIP, and dynamin-2 were expressed at the same level in patients as in normal individuals (*G*) (*lanes 4–12*).

These results give us a natural example that supports the importance of the complex formation of FBP17 with WASP, WIP, and dynamin-2 for the formation of podosomes and phagocytic cups.

DISCUSSION

Cell biological and structural analyses of the EFC domain of FBP17 have shown that the EFC domain binds to and deforms the plasma membrane (18, 22). It has previously been shown that the SH3 domain of FBP17 binds to N-WASP and dynamin in transfected cells (18, 21). However, physiologically important processes to which those activities of FBP17 contribute were unknown. Here, we have demonstrated that FBP17 recruits the WASP-WIP complex from the cytosol to the plasma membrane and that this recruitment is necessary for the formation of podosomes and phagocytic cups in macrophages. Our results suggest that FBP17 facilitates membrane deformation and actin polymerization induced by the WASP-WIP complex to occur simultaneously at the same membrane sites and that both are required for the formation of podosomes and phagocytic cups. This is supported by the observations that regulated actin polymerization is an essential process for the formation of podosomes (3) and phagocytic cups (29). Thus, FBP17 mediates a common molecular step in the formation of podosomes and phagocytic cups.

Macrophages have the ability to form both podosomes and phagocytic cups (Fig. 1, *A–D*). When macrophages having podosomes are stimulated with IgG-opsonized latex beads, the podosomes immediately disappear, and the phagocytic cups are formed at the site that the IgG beads attach. This observation indicates that the transition of the membrane structures occurs from podosomes to phagocytic cups. Macrophages migrate to sites of inflammation where they phagocytose pathogenic microbes and damaged tissue compounds and mediate local effector functions. Once macrophages encounter those materials at the site of inflammation, they stop migrating and phagocytose those materials. The transition of the macrophage functions occur from migration to phagocytosis. Podosomes and phagocytic cups are the essential membrane structures for migration and phagocytosis, respectively. Thus, the transition of the membrane structures from podosomes to phagocytic cups is essential and significant for the transition of the macrophage functions. Recently, two reports suggest that macrophage migration and phagocytosis include a common molecular mechanism to regulate actin cytoskeleton (40, 41). In this study, we identified a critical common molecular step mediated by FBP17 for the formation of podosomes and phagocytic cups, which are essential for migration and phagocytosis, respectively. In the future, elucidation of the molecular mechanisms underlying the transition would be intriguing.

It has been reported that dynamin-2 is also required for the formation of podosomes in transformed cells and osteoclasts (30–32) and phagocytic cups in a mouse macrophage cell line (33, 34) and that the FBP17-dynamin complex regulates the plasma membrane invagination (35). Our results suggest that FBP17 recruits dynamin-2 to the same site as membrane deformation and that this recruitment is also necessary for the formation of these structures (Figs. 3–5 and supplemental Fig. 6*C*). The formation of podosomes and phagocytic cups involves the process of the membrane protrusion (Fig. 1, *A–D*). The membrane protrusion requires the delivery of new membrane material (2). Our results, taken together with the above observations, suggest that dynamin-2 recruited by FBP17 to the plasma membrane probably plays an essential role in the formation of podosomes and phagocytic cups by regulating the recruitment of vesicles to the plasma membrane as new membrane material in macrophages.

Recently, the EFC domain of FBP17 was shown to bind strongly to the $PI(4,5)P_2$ (18, 22). On the other hand, it has been shown that $PI(4,5)P_2$ localizes at the podosomes in osteoclasts (36) and phagocytic cups (37, 38). These observations suggest that $PI(4,5)P_2$ is synthesized upon stimulation at the plasma membrane and plays an important role in the recruitment of FBP17 to the plasma membrane. Presumably, the $PI(4,5)P_2$ binding activity of the EFC domain is necessary for the localization of FBP17, and therefore, of the WASP-WIP complex and dynamin-2, at the sites where podosomes and phagocytic cups will form.

Role of FBP17 in the Podosome and Phagocytic Cup Formation

We suggest that the complex formation of FBP17 with WASP, WIP, and dynamin-2 at the plasma membrane is critical for the formation of podosomes and phagocytic cups (Figs. 1*G* and 3–5). In macrophages from WASP-deficient WAS patients, defects in the complex formation of FBP17 with WASP, WIP, and dynamin-2 impair the formation of podosomes and phagocytic cups (WAS1: 211delT (27); WAS2: 41–45delG(28) in Fig. 6), thereby reducing chemotaxis and phagocytosis by macrophages, which in turn would decrease the ability of host defense. The severity of WAS-associated symptoms was estimated and expressed as a score of 1–5. A score of 1 was assigned to patients with only thrombocytopenia and small platelets, and a score of 2 was assigned to patients with additional findings of mild, transient eczema or minor infections. Those with treatment-resistant eczema and recurrent infections despite optimal treatment received a score of 3 (mild WAS) or 4 (severe WAS). Regardless of the original score, if any patients then had autoimmune disease or malignancy, the score was changed to 5. The patients, WAS1 and WAS2, receive scores of 5 and 4, respectively. Both patients have the recurrent infections. We suggest that defective formation of podosomes and phagocytic cups in their macrophages (Fig. 6, *A–F*) reduces chemotaxis and phagocytosis, which are the critical processes to protect the body against infection, resulting in the recurrent infections. In addition, defective phagocytosis reduces the clearance of self-antigens such as apoptotic cells. This may cause the autoimmune diseases seen in WAS patients. In fact, Cohen *et al.* (39) recently reported that reduced clearance of apoptotic cells resulted in development of autoimmunity. Our findings therefore provide a potential mechanism for the recurrent infections and autoimmune diseases seen in WAS patients.

Acknowledgments—We thank Drs. M. Fukuda, R. C. Liddington, S. Courtneidge, A. Strongin (Burnham Institute for Medical Research), S. Grinstein (Hospital for Sich Children, Ontario, Canada), J. Condeelis (Albert Einstein Medical College), and P. De Camilli (Yale University) for critical reading of the manuscript and helpful discussion.

REFERENCES

1. Linder, S., and Aepfelbacher, M. (2003) *Trends Cell Biol.* **13,** 376–385
2. Linder, S. (2007) *Trends Cell Biol.* **17,** 107–117
3. Linder, S., Nelson, D., Weiss, M., and Aepfelbacher, M. (1999) *Proc. Natl. Acad. Sci. U. S. A.* **96,** 9648–9653
4. Tsuboi, S. (2007) *J. Immunol.* **178,** 2987–2995
5. Carman, C. V., Sage, P. T., Sciuto, T. E., Fuente, M. A. d. l., Geha, R. S., Ochs, H. D., Dvorak, H. F., Dvorak, A. M., and Springer, T. A. (2007) *Immunity* **26,** 784–797
6. Underhill, D. M., and Ozinsky, A. (2002) *Annu. Rev. Immunol.* **20,** 825–852
7. Leverrier, Y., and Ridley, A. J. (2001) *Curr. Biol.* **11,** 195–199
8. Wiskott, A. (1937) *Monatsschr. Kinderheilkd.* **68,** 212–216
9. Aldrich, R. A., Steinberg, A. G., and Campbell, D. C. (1954) *Pediatrics* **13,** 133–139
10. Notarangelo, L. D., Miao, C. H., and Ochs, H. D. (2008) *Curr. Opin. Hematol.* **15,** 30–36
11. Derry, J. M., Ochs, H. D., and Francke, U. (1994) *Cell* **78,** 635–644; Correction (1994) *Cell* **79,** 922
12. Lorenzi, R., Brickell, P. M., Katz, D. R., Kinnon, C., and Thrasher, A. J. (2000) *Blood* **95,** 2943–2946
13. Ramesh, N., Anton, I. M., Hartwig, J. H., and Geha, R. S. (1997) *Proc. Natl. Acad. Sci. U. S. A.* **94,** 14671–14676
14. Anton, I. M., de la Fuente, M. A., Sims, T. N., Freeman, S., Ramesh, N., Hartwig, J. H., Dustin, M. L., and Geha, R. S. (2002) *Immunity* **16,** 193–204
15. Chou, H. C., Anton, I. M., Holt, M. R., Curcio, C., Lanzardo, S., Worth, A., Burns, S., Thrasher, A. J., Jones, G. E., and Calle, Y. (2006) *Curr. Biol.* **16,** 2337–2344
16. Tsuboi, S., and Meerloo, J. (2007) *J. Biol. Chem.* **282,** 34194–34203
17. Tsuboi, S., Nonoyama, S., and Ochs, H. D. (2006) *EMBO Rep.* **7,** 506–511
18. Tsujita, K., Suetsugu, S., Sasaki, N., Furutani, M., Oikawa, T., and Takenawa, T. (2006) *J. Cell Biol.* **172,** 269–279
19. Chan, D. C., Bedford, M. T., and Leder, P. (1996) *EMBO J.* **15,** 1045–1054
20. Ho, H. Y., Rohatgi, R., Lebensohn, A. M., Le, M., Li, J., Gygi, S. P., and Kirschner, M. W. (2004) *Cell* **118,** 203–216
21. Kamioka, Y., Fukuhara, S., Sawa, H., Nagashima, K., Masuda, M., Matsuda, M., and Mochizuki, N. (2004) *J. Biol. Chem.* **279,** 40091–40099
22. Shimada, A., Niwa, H., Tsujita, K., Suetsugu, S., Nitta, K., Hanawa-Suetsugu, K., Akasaka, R., Nishino, Y., Toyama, M., Chen, L., Liu, Z. J., Wang, B. C., Yamamoto, M., Terada, T., Miyazawa, A., Tanaka, A., Sugano, S., Shirouzu, M., Nagayama, K., Takenawa, T., and Yokoyama, S. (2007) *Cell* **129,** 761–772
23. Auwerx, J. (1991) *Experientia (Basel)* **47,** 22–31
24. Kakimoto, T., Katoh, H., and Negishi, M. (2006) *J. Biol. Chem.* **281,** 29042–29053
25. Rebhun, J. F., Castro, A. F., and Quilliam, L. A. (2000) *J. Biol. Chem.* **275,** 34901–34908
26. Takayama, S., Krajewski, S., Krajewska, M., Kitada, S., Zapata, J. M., Kochel, K., Knee, D., Scudiero, D., Tudor, G., Miller, G. J., Miyashita, T., Yamada, M., and Reed, J. C. (1998) *Cancer Res.* **58,** 3116–3131
27. Jin, Y., Mazza, C., Christie, J. R., Giliani, S., Fiorini, M., Mella, P., Gandellini, F., Stewart, D. M., Zhu, Q., Nelson, D. L., Notarangelo, L. D., and Ochs, H. D. (2004) *Blood* **104,** 4010–4019
28. Imai, K., Morio, T., Zhu, Y., Jin, Y., Itoh, S., Kajiwara, M., Yata, J., Mizutani, S., Ochs, H. D., and Nonoyama, S. (2004) *Blood* **103,** 456–464
29. May, R. C., Caron, E., Hall, A., and Machesky, L. M. (2000) *Nat. Cell Biol.* **2,** 246–248
30. Ochoa, G. C., Slepnev, V. I., Neff, L., Ringstad, N., Takei, K., Daniell, L., Kim, W., Cao, H., McNiven, M., Baron, R., and De Camilli, P. (2000) *J. Cell Biol.* **150,** 377–389
31. McNiven, M. A., Baldassarre, M., and Buccione, R. (2004) *Front. Biosci.* **9,** 1944–1953
32. Bruzzaniti, A., Neff, L., Sanjay, A., Horne, W. C., De Camilli, P., and Baron, R. (2005) *Mol. Biol. Cell* **16,** 3301–3313
33. Gold, E. S., Underhill, D. M., Morrissette, N. S., Guo, J., McNiven, M. A., and Aderem, A. (1999) *J. Exp. Med.* **190,** 1849–1856
34. Tse, S. M., Furuya, W., Gold, E., Schreiber, A. D., Sandvig, K., Inman, R. D., and Grinstein, S. (2003) *J. Biol. Chem.* **278,** 3331–3338
35. Itoh, T., Erdmann, K. S., Roux, A., Habermann, B., Werner, H., and De Camilli, P. (2005) *Dev. Cell* **9,** 791–804
36. Chellaiah, M. A. (2005) *J. Biol. Chem.* **280,** 32930–32943
37. Botelho, R. J., Teruel, M., Dierckman, R., Anderson, R., Wells, A., York, J. D., Meyer, T., and Grinstein, S. (2000) *J. Cell Biol.* **151,** 1353–1368
38. Dewitt, S., Tian, W., and Hallett, M. B. (2006) *J. Cell Sci.* **119,** 443–451
39. Cohen, P. L., Caricchio, R., Abraham, V., Camenisch, T. D., Jennette, J. C., Roubey, R. A., Earp, H. S., Matsushima, G., and Reap, E. A. (2002) *J. Exp. Med.* **196,** 135–140
40. Brandt, D. T., Marion, S., Griffiths, G., Watanabe, T., Kaibuchi, K., and Grosse, R. (2007) *J. Cell Biol.* **178,** 193–200
41. Kato, M., Khan, S., d'Aniello, E., McDonald, K. J., and Hart, D. N. J. (2007) *J. Immunol.* **179,** 6052–6063
42. Calle, Y., Anton, I. M., Thrasher, A. J., and Jones, G. E. (2008) *J. Microsc. (Oxf.)* **231,** 494–505

Journal of the American College of Cardiology
© 2009 by the American College of Cardiology Foundation
Published by Elsevier Inc.

Vol. 53, No. 8, 2009
ISSN 0735-1097/09/$36.00
doi:10.1016/j.jacc.2008.11.014

PRE-CLINICAL RESEARCH

Prolonged Targeting of Ischemic/Reperfused Myocardium by Liposomal Adenosine Augments Cardioprotection in Rats

Hiroyuki Takahama, MD,*†‡ Tetsuo Minamino, MD, PHD,§ Hiroshi Asanuma, MD, PHD,† Masashi Fujita, MD, PHD,§ Tomohiro Asai, PHD,¶ Masakatsu Wakeno, MD, PHD,*†‡ Hideyuki Sasaki, MD,*†‡ Hiroshi Kikuchi, PHD,# Kouichi Hashimoto,** Naoto Oku, PHD,¶ Masanori Asakura, MD, PHD,† Jiyoong Kim, MD,† Seiji Takashima, MD, PHD,§ Kazuo Komamura, MD, PHD,|| Masaru Sugimachi, MD, PHD,|| Naoki Mochizuki, MD, PHD,*‡ Masafumi Kitakaze, MD, PHD, FACC†

Osaka, Shizuoka, and Tokyo, Japan

Objectives The purpose of this study was to investigate whether liposomal adenosine has stronger cardioprotective effects and fewer side effects than free adenosine.

Background Liposomes are nanoparticles that can deliver various agents to target tissues and delay degradation of these agents. Liposomes coated with polyethylene glycol (PEG) prolong the residence time of drugs in the blood. Although adenosine reduces the myocardial infarct (MI) size in clinical trials, it also causes hypotension and bradycardia.

Methods We prepared PEGylated liposomal adenosine (mean diameter 134 ± 21 nm) by the hydration method. In rats, we evaluated the myocardial accumulation of liposomes and MI size at 3 h after 30 min of ischemia followed by reperfusion.

Results The electron microscopy and ex vivo bioluminescence imaging showed the specific accumulation of liposomes in ischemic/reperfused myocardium. Investigation of radioisotope-labeled adenosine encapsulated in PEGylated liposomes revealed a prolonged blood residence time. An intravenous infusion of PEGylated liposomal adenosine (450 μg/kg/min) had a weaker effect on blood pressure and heart rate than the corresponding dose of free adenosine. An intravenous infusion of PEGylated liposomal adenosine (450 μg/kg/min) for 10 min from 5 min before the onset of reperfusion significantly reduced MI size (29.5 ± 6.5%) compared with an infusion of saline (53.2 ± 3.5%, $p < 0.05$). The antagonist of adenosine A_1, A_{2a}, A_{2b}, or A_3 subtype receptor blocked cardioprotection observed in the PEGylated liposomal adenosine-treated group.

Conclusions An infusion as PEGylated liposomes augmented the cardioprotective effects of adenosine against ischemia/reperfusion injury and reduced its unfavorable hemodynamic effects. Liposomes are promising for developing new treatments for acute MI. (J Am Coll Cardiol 2009;53:709–17) © 2009 by the American College of Cardiology Foundation

Liposomes are now widely used for drug delivery in cancer treatment to target specific organs actively or passively and to prevent the degradation of chemotherapy agents (1). However, the application of liposomes for cardiovascular diseases is still limited. In ischemic/reperfused myocardium, cellular permeability is enhanced and vascular endothelial integrity is disrupted (2,3), suggesting that nanoparticles

See page 718

*From the Department of Molecular Imaging in Cardiovascular Medicine, Osaka University Graduate School of Medicine, Osaka, Japan; †Department of Cardiovascular Medicine, National Cardiovascular Center, Osaka, Japan; ‡Department of Structural Analysis, Research Institute, National Cardiovascular Center, Osaka, Japan; §Department of Cardiovascular Medicine, Osaka University Graduate School of Medicine, Osaka, Japan; ||Department of Cardiovascular Dynamics, Research Institute, National Cardiovascular Center, Osaka, Japan; ¶Department of Medical Biochemistry, School of Pharmaceutical Sciences, University of Shizuoka, Shizuoka, Japan; #Daiichi Pharmaceutical Co., Tokyo, Japan; and the **Daiichi-Sankyo Pharmaceutical Co., Tokyo, Japan. Supported by a grant for Scientific Research and a grant for the Advancement of Medical Equipment from the Japanese Ministry of Health, Labor, and Welfare, as well as a grant from the Japan Cardiovascular Research Foundation.

Manuscript received September 4, 2008; revised manuscript received October 21, 2008, accepted November 3, 2008.

JACC Vol. 53, No. 8, 2009
February 24, 2009:709–17

Abbreviations and Acronyms

8-SPT = 8-(p-sulfophenyl) theophylline
EM = electron microscopy
MI = myocardial infarction
PEG = polyethylene glycol
RI = radioisotope
TTC = triphenyltetrazolium chloride

such as liposomes may be a promising drug delivery system for targeting damaged myocardium with cardioprotective agents. Additionally, coating liposomes with polyethylene glycol (PEG) prolongs their residence time in the circulation (1). Because enhanced microvascular permeability persists for at least 48 h after the occurrence of myocardial infarction (MI) (2), drugs delivered in PEGylated liposomes should be able to display their maximum beneficial effects on myocardial damage after MI.

Adenosine has multiple physiological functions that are mediated via the adenosine A_1, A_{2a}, A_{2b}, and A_3 receptors (4,5). Although large-scale clinical trials suggested the potential value of adenosine therapy for patients with acute MI (6,7), this agent has an extremely short half-life (1 to 2 s) and causes hypotension and bradycardia because of vasodilatory and negative chronotropic effects (4). Because a high dose of adenosine is required to exert cardioprotective effects, it is difficult to use clinically because of the associated hemodynamic consequences. Therefore, we hypothesized that adenosine encapsulated in PEGylated liposomes would cause less hemodynamic disturbance and might also specifically accumulate in ischemic/reperfused myocardium, leading to augmented cardioprotective effects. To test this hypothesis, we created PEGylated liposomal adenosine by the hydration method and investigated: 1) whether liposomal adenosine accumulated in ischemic/reperfused myocardium and prolonged blood residence time; 2) whether liposomal adenosine caused less severe hypotension and bradycardia than free adenosine; and 3) which adenosine receptor subtype was involved in mediating the cardioprotective effects of liposomal adenosine against ischemia/reperfusion injury.

Methods

Materials. The materials for preparing PEGylated liposomes, including hydrogenated soy phosphatidyl choline (HSPC), 1,2-distearoyl-sn-glycero-3-phosphoethanolamine-n-[methoxy (polyethylene glycol)-2000] (DSPE-PEG2000), and cholesterol were obtained from Nissei Oil Co., Ltd. (Tokyo, Japan) and Wako Pure Chemical Co., Ltd. (Osaka, Japan). [^{3}H]-adenosine was purchased from Daiichi Pure Chemicals Co., Ltd. (Tokyo, Japan). Other materials were obtained from Sigma (St. Louis, Missouri), including 8-(*p*-sulfophenyl)theophylline (8-SPT; a nonselective adenosine receptor antagonist), 1,3-diethyl-8-phenylxanthine (DPCPX; a selective adenosine A_1 receptor antagonist), 5-amino-7-(phenylethyl)-2-(2-furyl)-pyrazolo[4,3-e]-1,2,4-triazolo[1,5-c] pyrimidine (SCH58261; a selective adenosine A_{2a} receptor antagonist), 8-[4-[((4-cyanophenyl)carbamoylmethyl) oxy]phenyl]-1, 3-di(n-propyl)xanthine (MRS1754; a selective adenosine A_{2b} receptor antagonist), and 5-propyl-2-ethyl-4-propyl-3-(ethylsulfanylcarbonyl)-6-phenylpyridine-5-carboxylate (MRS1523, a selective adenosine A_3 receptor antagonist).

Animals. Male Wistar rats (9 weeks old and weighing 250 to 310 g, Japan Animals, Osaka, Japan) were used. The animal experiments were approved by the National Cardiovascular Center Research Committee and were performed according to institutional guidelines.

Preparation of PEGylated liposomes. The PEGylated liposomes were prepared by the hydration method. Briefly, adenosine was added to the lipid solution. After mixture of lipid and adenosine, DSPE-PEG2000 was added and incubated. The final composition of PEGylated liposomes was HSPC:cholesterol:DSPE-PEG2000 = 6.0:4.0:0.3 (molar ratio). After ultracentrifugation several times, the pellet of liposomal adenosine was resuspended in sodium lactate at each required concentration for use in the experimental protocols. Some samples of final liposomal adenosine were disrupted by dilution with 50% methanol (1.5 ml per 30-μl of liposomes). After 10 min of ultracentrifugation, the concentration of adenosine in the supernatant was measured by high-performance liquid chromatography.

To prepare fluorescent-labeled liposomes, 0.5 mol% tetramethylrhodamine isothiocyanate (rhodamine) was added to the lipid mixture. To prepare radioisotope (RI)-labeled adenosine encapsulated in liposomes, [^{3}H]-radiolabeled adenosine (Daiichi Pure Chemicals, Tokyo, Japan) was diluted with free adenosine and was encapsulated in liposomes as described above.

Characterization of PEGylated liposomal adenosine. The characterization of the liposomes was performed by the dynamic scatter analysis (Zetasizer Nano ZS, Malvern, Worcestershire, United Kingdom). The analyses were performed 10 times per sample, and results represented analyses of 4 independent experiments.

Experimental protocols. PROTOCOL 1: EFFECTS OF PEGYLATED LIPOSOMAL ADENOSINE ON HEMODYNAMICS IN RATS. Rats were anesthetized with intraperitoneal sodium pentobarbital (50 mg/kg). Catheters were advanced into a femoral artery and vein for the measurement of systemic blood pressure and infusion of drugs, respectively. Both blood pressure and heart rate were monitored continuously during the study using a Power Lab (AD Instruments, Castle Hill, Australia). After hemodynamics became stable, we intravenously administered empty PEGylated liposomes (n = 8), free adenosine (n = 8), or PEGylated liposomal adenosine (n = 8) for 10 min. Either PEGylated liposomal or free adenosine was infused at an initial dose of 225 μg/kg/min (0.1 ml/min) for 10 min. After a 5-min interval, either PEGylated liposomal adenosine or free adenosine was infused at 450 μg/kg/min (0.1 ml/min) for 10 min. In the same manner, PEGylated liposomal adenosine or free adenosine was then infused at 900 μg/kg/min (0.1 ml/min).

PROTOCOL 2: EFFECTS OF PEGYLATED LIPOSOMAL ADENOSINE ON INFARCT SIZE IN RATS. The MI was induced by transient ligation of the left coronary artery as described previously (8). In the first series of experiments, to examine the dose-dependent effects of liposomal adenosine on MI size, PEGylated liposomal adenosine was infused intravenously at 50, 150, or 450 μg/kg/min for a 10-min period starting from 5 min before the onset of reperfusion. In the second series of experiments, to determine the adenosine receptor subtype involved in cardioprotective effects by the liposomal adenosine, the antagonist of adenosine subtype receptor was intravenously injected as a bolus followed by the infusion of liposomal adenosine for 10 min. The MI size was evaluated at 3 h after the start of reperfusion. The doses of adenosine receptor subtype antagonists were determined according to the previous reports (9–11).

Measurement of infarct size. At 3 h after the onset of reperfusion, the area at risk and the infarcted area were determined by Evans blue and triphenyltetrazolium chloride (TTC) staining, respectively, as previously described (8). Infarct size was calculated as [infarcted area/area at risk] × 100(%) in a blind manner. The area at risk was composed of border (TTC staining) and infarcted (TTC nonstaining) areas.

Electron microscopy (EM). Myocardial samples for EM were obtained from the central and peripheral areas in ischemic/reperfused myocardium, which roughly corresponded to the infarcted and border areas, respectively, after the left coronary artery was occluded for 30 min of ischemia followed by 3 h of reperfusion. Samples were prepared as previously reported (12). Liposomes, whose major membrane component is unsaturated phospholipids, were visualized as homogenous dark dots with a diameter of 100 to 150 nm (13).

Accumulation of fluorescent-labeled PEGylated liposomes in ischemic/reperfused myocardium. Unlabeled or fluorescent-labeled PEGylated liposomes were infused intravenously at a dose of 0.1 ml/min as liposomal adenosine was infused in protocol 2. At 3 h after reperfusion, hearts were quickly removed and cut into 4 sections parallel to the axis from base to apex. Then ex vivo bioluminescence imaging was performed with an Olympus OV 100 imaging system (Olympus, Tokyo, Japan) and signals were quantified using WASABI quantitative software (Hamamatsu Photonics K.K., Shizuoka, Japan). Fluorescent intensity in the region of interest was measured as previously reported (14). Control intensity indicated the fluorescent intensity in the nonischemic area of the individual rat.

Time-course changes of free and PEGylated liposomal RI-labeled adenosine in plasma and myocardium. Free or PEGylated liposomal [^{3}H]-adenosine (83 kBq per rat) was infused intravenously at a dose of 0.1 ml/min as liposomal adenosine was infused in protocol 2. At the time indicated, rat hearts were harvested for counting of radioactivity (LSC-3100, Aloka Co., Tokyo, Japan). Results are expressed as a percentage of the injected dose per 1 ml of blood or 1 g of wet tissue weight.

Statistical analysis. The parameters of the liposomes were expressed as the average ± SD, whereas other data were expressed as the average ± SEM. Comparison of time-course changes in hemodynamic parameters between groups was performed by 2-way repeated-measures analysis of variance (ANOVA) followed by a post-hoc Bonferroni test. For comparison of RI activity between groups, statistical analysis was done with the Mann-Whitney *U* test. To address the differences in infarct size among groups, we performed a nonparametric (Kruskal-Wallis) test followed by evaluation with the Mann-Whitney *U* test. Resulting p values were corrected according to the Bonferroni method. To compare parameters of liposomes, an unpaired *t* test was performed. In all analyses, $p < 0.05$ was considered to indicate statistical significance.

Results

Characterization of liposomes by dynamic light scatter analysis. The dynamic light scatter analysis showed no significant difference in mean diameter, polydispersity index, or zeta-potential distribution between empty and adenosine-loaded PEGylated liposomes (Table 1).

Liposomes in ischemic/reperfused myocardium. The EM revealed the intact vascular endothelial cells and cardiomyocytes in the nonischemic myocardium (Figs. 1A and 1B). There were no homogenous dark dots indicating liposomes in the nonischemic myocardium of rats that received either saline (Fig. 1A) or liposomes (Fig. 1B). In the border area, many homogenous dark dots indicating liposomes were accumulated in rats that received liposomes, but not saline (Figs. 1C and 1D). In this area, significant structural damage was not observed in endothelium, but slight swelling of mitochondria was often observed. In the infarcted area, numerous liposomes were detected in rats that received liposomes, but not saline (Figs. 1E and 1F). In this area, the disrupted endothelial integrity and marked swelling of mitochondria were often observed.

Table 1 Characterization of Liposomes by Dynamic Light Scatter Analysis

	Mean Diameter (nm)	Polydispersity Index	Zeta Potential (mV)
PEGylated liposomes (empty liposomes)	126 ± 12	0.035 ± 0.003	−1.7 ± 0.4
PEGylated liposomal adenosine	134 ± 21	0.094 ± 0.002	−2.3 ± 1.1

Results represented analysis of 4 independent experiments. Values are expressed as mean ± SD.
PEG = polyethylene glycol.

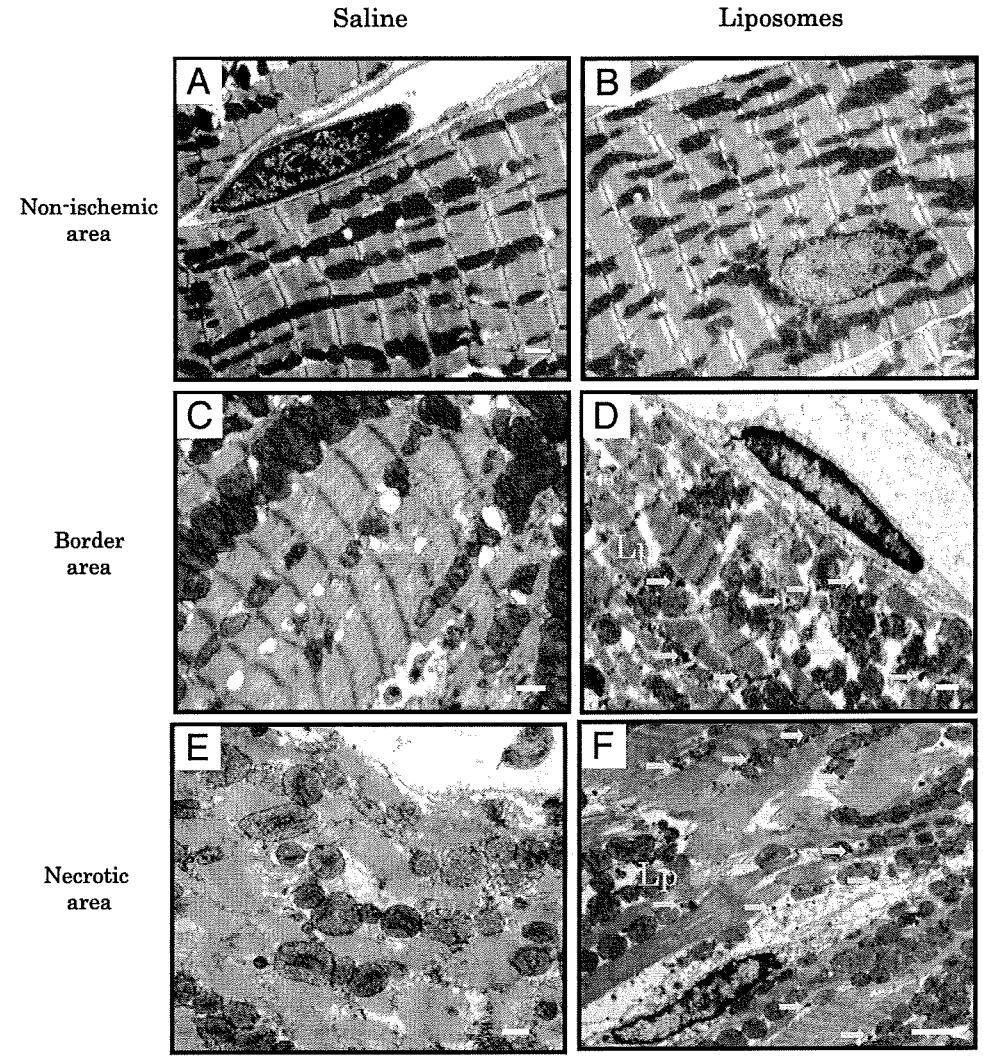

Figure 1 **Liposomes in Ischemic/Reperfused Myocardium**

(A, B) Representative electron micrographs of the nonischemic area in rats that received saline **(A)** or liposomes (Lp) **(B)**. **(C, D)** Representative electron micrographs of border area at 3 h after myocardial infarction (MI). Many **dark dots** accumulated in this area in the rat that received liposomes but not saline. **(E, F)** Representative electron micrographs of infarcted areas at 3 h after MI. Numerous **dark dots** accumulated in this area in the rat that received liposomes but not saline. Scale bars represent 1 μm.

Fluorescent-labeled PEGylated liposomes in ischemic/reperfused myocardium. Quantitative analysis by bioluminescence ex vivo bioluminescene imaging revealed that the target to control fluorescent intensity ratio was higher in the border (noninfarcted area at risk) as well as infarcted areas compared with a nonischemic one, suggesting that fluorescent-labeled liposomes were accumulated in the border as well as infarcted areas. Since there was no high-intensity area when unlabeled liposomes were infused, it was suggested that this was not a nonspecific phenomenon to MI by the ex vivo bioluminescence imaging system (Fig. 2). The Evans blue staining was unrelated to the fluorescence intensity (data not shown).

Plasma radioactivity of RI-labeled adenosine was markedly higher in the PEGylated liposomal adenosine group at 10 min and 3 h after the intravenous infusion than in the free adenosine group (Fig. 3A). Encapsulation within PEGylated liposomes also augmented the accumulation of adenosine in ischemic/reperfused myocardium compared with that of free adenosine (Fig. 3B).

Hemodynamic effects of PEGylated liposomal adenosine. Baseline hemodynamic parameters did not differ among the groups. An intravenous infusion of free adenosine at doses of 225, 450, and 900 μg/kg/min decreased the mean blood pressure by 14.8%, 25.4%, and 33.7%, respectively, compared with the effect of empty PEGylated lipo-

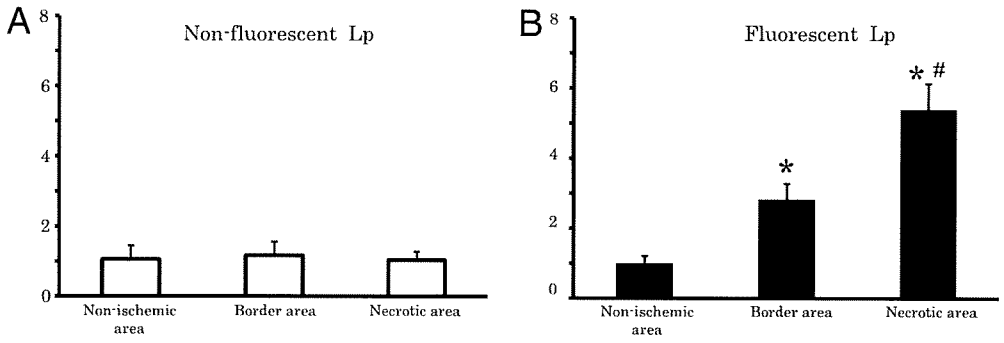

Figure 2 **Detection of Fluorescence-Labeled PEGylated Liposomes in Ischemic/Reperfused Myocardium**

Quantitative analysis of target-to-control fluorescent intensity ratio for each area in rats (n = 3 each group) that received nonfluorescent **(A)** or fluorescent **(B)** liposomes. The values of bioluminescence signals in the border and infarcted areas were expressed as the fold to that of the each nonischemic area. Values are expressed as the mean ± SEM (error bars). *p < 0.05 versus nonischemic areas. #p < 0.05 versus border areas.

somes. In contrast, the intravenous infusion of PEGylated liposomal adenosine at a dose of either 225 or 450 μg/kg/min did not significantly alter mean blood pressure (Fig. 4). Changes of the heart rate after infusion of PEGylated liposomal adenosine or free adenosine were similar to those observed for mean blood pressure (Fig. 4).

Effects of PEGylated liposomal adenosine on MI size. Baseline hemodynamic parameters were similar among all of the groups (Table 2). Intravenous infusion of free adenosine for 10 min reduced both the blood pressure and the heart rate, although these parameters returned to baseline within 5 min of ceasing infusion (Table 2). In contrast, hemodynamic parameters of the other groups were not altered (Table 2). The area at risk in the control group (61 ± 3%) did not differ compared with those of other groups that received liposomal adenosine. Intravenous infusion of PEGylated liposomal adenosine caused a dose-dependent decrease of MI size compared with that in the control group, whereas intravenous infusion of empty PEGylated liposomes or free adenosine did not (Fig. 5B).

The bolus injection of adenosine receptor antagonist did not alter the hemodynamic parameters (Table 3). The area at risk in the liposomal adenosine group (58 ± 3%) did not differ compared with those of other groups that received adenosine receptor antagonist. Infusion of 8-SPT, a nonspecific adenosine receptor antagonist, blunted the cardioprotective effect of liposomal adenosine (Fig. 6B). Furthermore, the infusion of the adenosine A_1, A_{2a}, A_{2b}, or A_3 receptor antagonist also blunted cardioprotective effects of liposomal adenosine (Fig. 6B). Infusion of 8-SPT alone did not significantly affect myocardial infarct size compared with the control (52 ± 5%, n = 4).

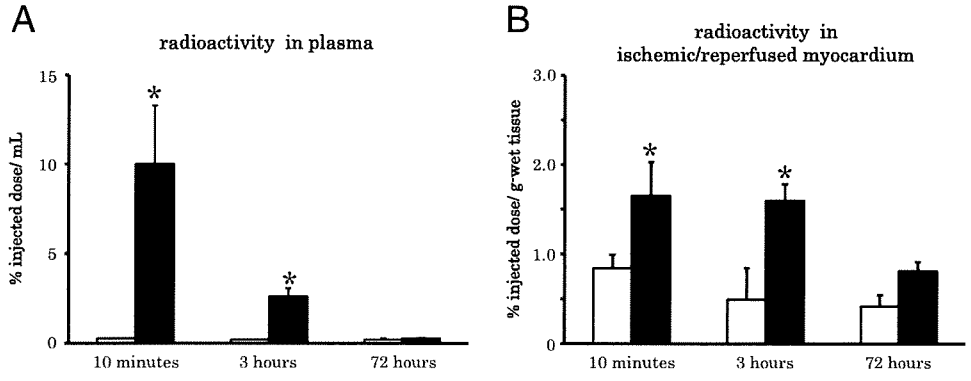

Figure 3 **Radioisotope-Labeled Adenosine in Plasma and Ischemic/Reperfused Myocardium**

(A) Changes in plasma radioactivity after infusion of radioisotope-labeled adenosine. **Solid and open bars** indicate the PEGylated liposomal adenosine and free adenosine groups, respectively (n = 4 each). In the PEGylated liposomal adenosine group, plasma radioactivity was markedly higher than in the free adenosine group. **(B)** Changes in radioactivity in ischemic/reperfused myocardium. **Solid and open bars** indicate the PEGylated liposomal adenosine and free adenosine groups, respectively (n = 4 each). In the PEGylated liposomal adenosine group, myocardial radioactivity was markedly higher than in the free adenosine group. Values are expressed as the mean ± SEM (error bars). *p < 0.05 versus the free adenosine group at the corresponding time.

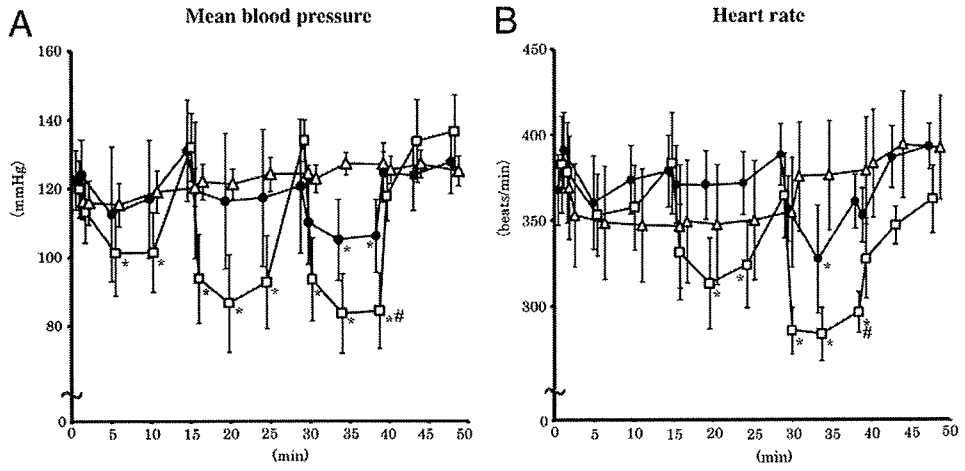

Figure 4 **Hemodynamic Effects of PEGylated Liposomal Adenosine**

Changes in the mean blood pressure **(A)** and heart rate **(B)** after intravenous infusion of various doses of empty PEGylated liposomes **(triangles)**, PEGylated liposomal adenosine **(circles)**, or free adenosine **(squares)** (n = 8 each). Values are expressed as the mean ± SEM. *p < 0.05 versus baseline at the corresponding group. #p < 0.05 versus PEGylated liposomes.

Discussion

In the present study, EM, bioluminescence ex vivo imaging, and fluorescent analysis revealed the accumulation of liposomes in the border (noninfarcted areas at risk) as well as infarcted ones, but not nonischemic myocardium, at 3 h after MI. These findings suggested that liposomes could specifically accumulate in ischemic/reperfused myocardium. Interestingly, EM revealed the existence of liposomes at sites where endothelial integrity was still morphologically maintained. Endothelial dysfunction such as enhanced permeability is induced by ischemic insult without morphological endothelial disruption (3,15). Enhanced permeability might lead to the accumulation of liposomes in the border as well as infarcted area, which will contribute to salvage the ischemic/reperfused myocardium. However, further investigation will be needed to determine the precise mechanism by which liposomes accumulate in ischemic/reperfused myocardium.

Analysis using RI-labeled adenosine encapsulated in liposomes revealed that plasma radioactivity was markedly higher in the PEGylated liposomal adenosine group compared with the free adenosine group. This indicates that encapsulation of adenosine by PEGylated liposomes considerably prolonged its residence time in the circulation and delayed its degradation. Consistent with the histological data, RI-labeled adenosine also showed preferential accumulation in ischemic/reperfused myocardium.

Table 2 **Effects of Liposomal Adenosine on Hemodynamic Parameters**

		Ischemia				Reperfusion	
	Baseline	0 min	15 min	25 min	30 min	5 min	10 min
Mean blood pressure (mm Hg)							
Saline	122 ± 5	102 ± 10	108 ± 7	107 ± 9	108 ± 7	105 ± 9	104 ± 9
Vehicle	127 ± 4	109 ± 8	108 ± 7	111 ± 9	111 ± 5	105 ± 5	103 ± 5
Free-Ado	124 ± 8	115 ± 8	111 ± 5	109 ± 4	66 ± 4*	62 ± 4*	112 ± 6
Lp-Ado 50 μg/kg/min	121 ± 5	106 ± 6	105 ± 6	110 ± 10	102 ± 6	101 ± 6	104 ± 4
Lp-Ado 150 μg/kg/min	122 ± 3	107 ± 6	107 ± 6	109 ± 11	105 ± 6	100 ± 6	103 ± 4
Lp-Ado 450 μg/kg/min	124 ± 3	104 ± 6	105 ± 6	107 ± 5	102 ± 6	99 ± 6	104 ± 4
Heart rate (beats/min)							
Saline	363 ± 22	366 ± 19	369 ± 14	413 ± 22	372 ± 12	372 ± 16	371 ± 14
Vehicle	363 ± 32	363 ± 6	383 ± 6	396 ± 25	367 ± 6	374 ± 7	372 ± 7
Free-Ado	360 ± 18	361 ± 17	384 ± 13	379 ± 18	305 ± 11*	293 ± 13*	356 ± 14
Lp-Ado 50 μg/kg/min	378 ± 19	386 ± 21	366 ± 12	376 ± 12	367 ± 19	369 ± 9	377 ± 17
Lp-Ado 150 μg/kg/min	388 ± 27	376 ± 20	371 ± 14	377 ± 13	378 ± 16	373 ± 16	369 ± 17
Lp-Ado 450 μg/kg/min	368 ± 17	376 ± 21	361 ± 13	386 ± 15	368 ± 15	363 ± 6	367 ± 7

Values are expressed as mean ± SEM. *p < 0.05 versus baseline.
Free-Ado = free adenosine; Lp-Ado = PEGylated liposomal adenosine; PEG = polyethylene glycol; vehicle = PEGylated liposomes.

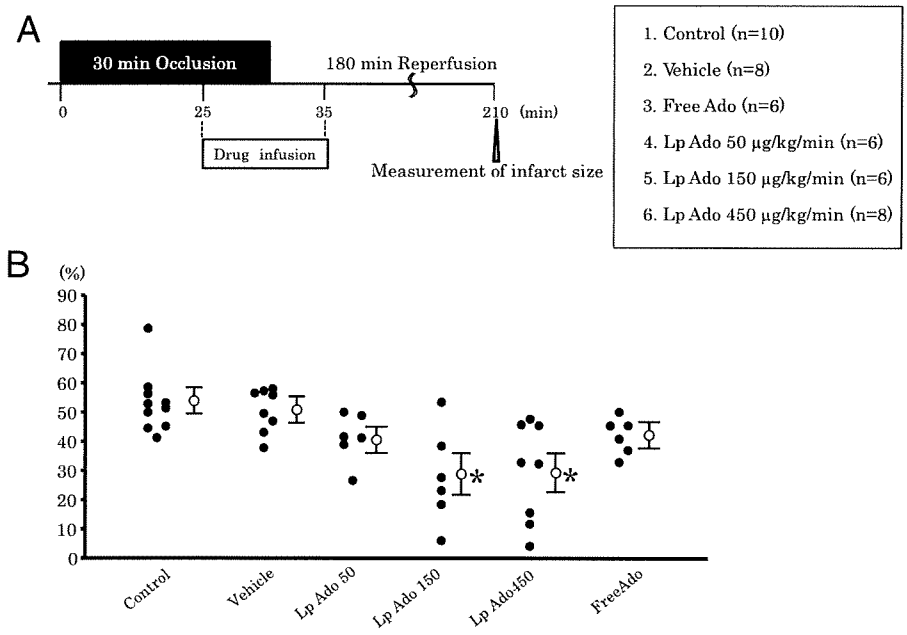

Figure 5 Dose-Dependent Effects of PEGylated Liposomal Adenosine on Myocardial Infarct Size

(A) Protocol showing the timing of infusion of PEGylated liposomal adenosine and of infarct size measurement. **(B)** Myocardial infarct size. Values are expressed as mean ± SEM (error bars). *p < 0.05 versus the control group. Free-Ado = free adenosine; Lp-Ado = PEGylated liposomal adenosine; Vehicle = PEGylated liposomes.

Furthermore, this study showed that PEGylated liposomal adenosine had a weaker effect on the blood pressure and heart rate than free adenosine. Thus, encapsulating adenosine in PEGylated liposomes attenuated its vasodilatory and negative chronotropic effects, presumably by reducing the amount of circulating free adenosine. However, the changes of hemodynamic parameters in this in vivo model suggested that significant release of adenosine from PEGylated liposomes would still occur if a large dose of liposomal adenosine (e.g., 900 μg/kg/min) were administered. Thus, further investigation of the in vivo pharmacodynamics of PEGylated liposomal adenosine is needed.

An intravenous infusion of PEGylated liposomal adenosine at the maximum dose that did not disturb hemodynamic parameters for 10 min before reperfusion reduced MI size in a dose-dependent manner, and this improvement was blocked by 8-SPT, a nonselective adenosine receptor antagonist. These findings suggest that adenosine released from liposomes acts via an adenosine receptor-dependent pathway. One possible mechanism by which PEGylated lipo-

Table 3 Effects of Adenosine Receptor Antagonist on Hemodynamic Parameters

		Ischemia				Reperfusion	
	Baseline	0 min	15 min	25 min	30 min	5 min	10 min
Mean blood pressure (mm Hg)							
Lp-Ado + 8SPT	120 ± 6	113 ± 4	112 ± 6	112 ± 5	107 ± 6	102 ± 8	109 ± 7
Lp-Ado + DPCPX	130 ± 6	105 ± 4	121 ± 4	100 ± 10	122 ± 6	120 ± 6	111 ± 4
Lp-Ado + SCH58261	132 ± 2	98 ± 12	99 ± 8	110 ± 8	118 ± 10	113 ± 10	109 ± 6
Lp-Ado + MRS1754	130 ± 3	95 ± 12	106 ± 8	105 ± 10	100 ± 10	96 ± 10	99 ± 7
Lp-Ado + MRS1523	130 ± 2	109 ± 8	104 ± 8	105 ± 9	100 ± 9	101 ± 10	104 ± 6
Heart rate (beats/min)							
Lp-Ado + 8SPT	404 ± 17	385 ± 10	374 ± 8	396 ± 8	389 ± 9	383 ± 8	385 ± 9
Lp-Ado + DPCPX	396 ± 24	380 ± 11	399 ± 9	398 ± 12	385 ± 9	382 ± 9	380 ± 7
Lp-Ado + SCH58261	393 ± 14	399 ± 15	381 ± 9	395 ± 15	376 ± 9	373 ± 9	385 ± 7
Lp-Ado + MRS1754	398 ± 14	392 ± 11	401 ± 9	379 ± 15	378 ± 9	374 ± 9	377 ± 7
Lp-Ado + MRS1523	396 ± 9	390 ± 11	390 ± 11	392 ± 10	373 ± 9	391 ± 7	388 ± 11

Values were expressed as mean ± SEM. *p < 0.05 versus baseline.
Lp-Ado = PEGylated liposomal adenosine; PEG = polyethylene glycol; Vehicle = PEGylated liposomes.

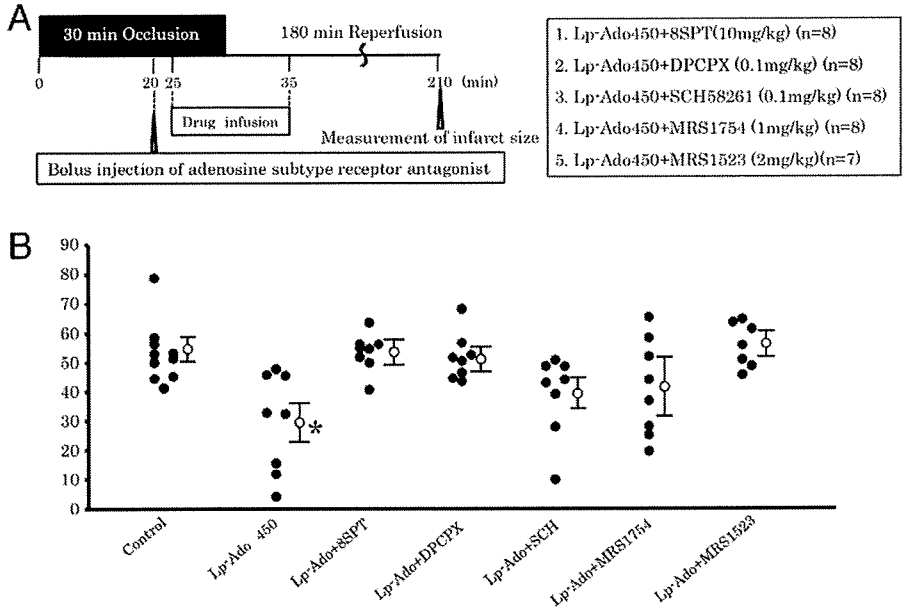

Figure 6 **Effects of Adenosine Receptor Antagonists on Myocardial Infarct Size**

(A) Protocol showing the timing of infusion of PEGylated liposomal adenosine and bolus injection adenosine receptor antagonists. **(B)** Myocardial infarct size. Values are expressed as the mean ± SEM (error bars). *$p < 0.05$ versus the control group. The abbreviations for adenosine antagonists were described in the text. Abbreviations as in Figure 5.

somes could augment cardioprotective effects of liposomal adenosine with minimum effects on hemodynamic parameters is the enhanced accumulation of PEGylated liposomal adenosine in ischemic/reperfused myocardium, which could augment various beneficial actions such as preventing calcium overload in the myocardium (5). The prolonged persistence of PEGylated liposomal adenosine would also increase its beneficial effect on ischemic/reperfused myocardium. Although continuous high-dose, long-term infusion of free adenosine was reported to reduce infarct size in rats (16), the present study did not confirm such a cardioprotective effect, probably because the total dose of free adenosine that we used was not high enough.

We found that myocardial infarct size in the group that received PEGylated liposomal adenosine with the antagonist of adenosine A_1, A_{2a}, A_{2b}, or A_3 subtype receptor was no different from the control group, indicating that every adenosine subtype receptor could possibly play a role in mediating cardioprotection by liposomal adenosine and that it was difficult to identify one particular subtype in the present study. Numerous studies reported that A_1, A_{2a}, A_{2b}, and A_3 receptors have been involved in cardioprotection against ischemia/reperfusion injury, and it remains controversial which adenosine subtype receptor is most responsible for cardioprotection (17–20). Furthermore, because the adenosine receptor antagonists used in the present study had some nonspecific effects, future investigation will be needed to examine the precise role of each adenosine receptor subtype using genetically engineered mice.

Because liposomal adenosine infused during reperfusion could reduce MI size, this agent could be a candidate for the adjunctive therapy of patients with acute MI. Importantly, adenosine is currently used for the diagnosis of ischemic heart disease and PEGylated liposomes are used to deliver anticancer agents (21). Thus, it should not be difficult to introduce PEGylated liposomal adenosine into clinical practice. Finally, PEGylated liposomes may provide a useful drug delivery system for targeting ischemic/reperfused myocardium with other agents.

Acknowledgments

The authors thank Akiko Ogai and Yoko Nakano for their excellent technical assistance; Motohide Takahama, Hiroyuki Hao, and Hatsue Ishibashi-Ueda for advice about the electron microscopy figure; and Syunichi Kuroda and Takashi Matsuzaki for assistance with bioluminescence imaging.

Reprint requests and correspondence: Dr. Tetsuo Minamino, Department of Cardiovascular Medicine, Osaka University Graduate School of Medicine, 2-2 Yamadaoka, Suita, Osaka 565-0871, Japan. E-mail: minamino@medone.med.osaka-u.ac.jp.

REFERENCES

1. Papahadjopoulos D, Allen TM, Gabizon A, et al. Sterically stabilized liposomes: improvements in pharmacokinetics and antitumor therapeutic efficacy. Proc Natl Acad Sci U S A 1991;24:11460–4.

2. Horwitz LD, Kaufman D, Keller MW, Kong Y. Time course of coronary endothelial healing after injury due to ischemia and reperfusion. Circulation 1994;90:2439–47.
3. Dauber IM, Van Benthuysen KM, McMurtry IF, et al. Functional coronary microvascular injury evident as increased permeability due to brief ischemia and reperfusion. Circ Res 1990;66:986–98.
4. Forman MB, Stone GW, Jackson EK. Role of adenosine as adjunctive therapy in acute myocardial infarction. Cardiovasc Drug Rev 2006;24:116–47.
5. Mubagwa K, Flameng W. Adenosine, adenosine receptors and myocardial protection: an updated overview. Cardiovasc Res 2001;52:25–39.
6. Mahaffey KW, Pume JA, Barbagelata NA, et al. Adenosine as an adjunct to thrombolytic therapy for acute myocardial infarction: results of a multicenter, randomized, placebo-controlled trial: the Acute Myocardial Infarction STudy of ADenosine (AMISTAD) trial. J Am Coll Cardiol 1999;34:1711–20.
7. Ross AM, Gibbons RJ, Stone GW, Kloner RA, Alexander RW, for the AMISTAD-II ÅInvestigators. A randomized, double-blinded, placebo-controlled multicenter trial of adenosine as an adjunct to reperfusion in the treatment of acute myocardial infarction (AMISTAD-II). J Am Coll Cardiol 2005;45:1775–80.
8. Bullard AJ, Govewalla P, Yellon DM. Erythropoietin protects the myocardium against reperfusion injury in vitro and in vivo. Basic Res Cardiol 2005;100:397–403.
9. Hannon JP, Tigani B, Wolber C, et al. Evidence for an atypical receptor mediating the augmented bronchoconstrictor response to adenosine induced by allergen challenge in activity sensitized Brown Norway rats. Br J Pharmacol 2002;135:685–96.
10. Kin H, Zatta AJ, Lofye MT, et al. Postconditioning reduces infarct size via adenosine receptor activation by endogenous adenosine. Cardiovasc Res 2005;67:124–33.
11. Hinschen AK, RoseMeyer RB, Headrick JP. Adenosine receptor subtypes mediating coronary vasodilation in rat hearts. J Cardiovasc Pharmacol 2003;41:73–80.
12. Kaeffeer N, Richard V, Francois A, Lallemand F, Henry JP, Thuillez C. Preconditioning prevents chronic reperfusion-induced coronary endothelial dysfunction in rats. Am J Physiol 1996;271:H842–9.
13. M Shimizu, Miwa K, Hashimoto Y, Goto A. Encapsulating of chicken egg yolk immunoglobulin G (IgY) by liposomes. Biosci Biotechnol Biochem 1993;57:1445–9.
14. Kasuya T, Jung J, Kadoya H, et al. In vivo delivery of bionanocapsules displaying phaseolus vulgaris agglutinin-L(4) isolectin to malignant tumors overexpressing N-acetylglucosaminlyltransferase V. Hum Gene Ther 2008;19:887–95.
15. Kim YD, Fomsgaard JS, Heim KF, et al. Brief ischemia-reperfusion induces stunning of endothelium in canine coronary artery. Circulation 1992;85:1473–82.
16. Canyon SJ, Dobson GP. Protection against ventricular arrhythmias and cardiac death using adenosine and lidocaine during regional ischemia in the in vivo rat. Am J Physiol Heart Circ Physiol 2004;287:H1286–95.
17. Yaar R, Jones MR, Chen JF, Ravid K. Animal models for the study of adenosineÅreceptor function. J Cell Physiol 2005;202:9–20.
18. Norton ED, Jackson EK, Turner MB, Virmani R, Forman MB. The effects of intravenous infusions of selective adenosine A_1-receptor and A_2-receptor agonists on myocardial reperfusion injury. Am Heart J 1992;123:332–8.
19. Xu Z, Mueller RA, Park SS, Boysen PG, Cohen MV, Downey JM. Cardioprotection with adenosine A_2 receptor activation at reperfusion. J Cardiovasc Pharmacol 2005;46:794–802.
20. Vinten-Johansen J. Postconditioning: a mechanical maneuver that triggers biological and molecular cardioprotective responses to reperfusion. Heart Fail Rev 2007;12:235–344.
21. Lasic DD. Doxorubicin in sterically stabilized liposomes. Nature 1996;380:561–2.

Key Words: myocardial infarction ▪ liposome ▪ drug delivery system ▪ adenosine.

Circulation Research
JOURNAL OF THE AMERICAN HEART ASSOCIATION

American Heart Association®
Learn and Live℠

Activating Transcription Factor 3 Constitutes a Negative Feedback Mechanism That Attenuates Saturated Fatty Acid/Toll-Like Receptor 4 Signaling and Macrophage Activation in Obese Adipose Tissue

Takayoshi Suganami, Xunmei Yuan, Yuri Shimoda, Kozue Uchio-Yamada, Nobutaka Nakagawa, Ibuki Shirakawa, Takako Usami, Takamitsu Tsukahara, Keizo Nakayama, Yoshihiro Miyamoto, Kazuki Yasuda, Junichiro Matsuda, Yasutomi Kamei, Shigetaka Kitajima and Yoshihiro Ogawa

Circ. Res. 2009;105;25-32; originally published online May 28, 2009;
DOI: 10.1161/CIRCRESAHA.109.196261
Circulation Research is published by the American Heart Association. 7272 Greenville Avenue, Dallas, TX 72514
 Print ISSN: 0009-7330. Online ISSN: 1524-4571

Activating Transcription Factor 3 Constitutes a Negative Feedback Mechanism That Attenuates Saturated Fatty Acid/Toll-Like Receptor 4 Signaling and Macrophage Activation in Obese Adipose Tissue

Takayoshi Suganami, Xunmei Yuan, Yuri Shimoda, Kozue Uchio-Yamada, Nobutaka Nakagawa, Ibuki Shirakawa, Takako Usami, Takamitsu Tsukahara, Keizo Nakayama, Yoshihiro Miyamoto, Kazuki Yasuda, Junichiro Matsuda, Yasutomi Kamei, Shigetaka Kitajima, Yoshihiro Ogawa

Abstract—Obese adipose tissue is markedly infiltrated by macrophages, suggesting that they may participate in the inflammatory pathways that are activated in obese adipose tissue. Evidence has suggested that saturated fatty acids released via adipocyte lipolysis serve as a naturally occurring ligand that stimulates Toll-like receptor (TLR)4 signaling, thereby inducing the inflammatory responses in macrophages in obese adipose tissue. Through a combination of cDNA microarray analyses of saturated fatty acid–stimulated macrophages in vitro and obese adipose tissue in vivo, here we identified activating transcription factor (ATF)3, a member of the ATF/cAMP response element-binding protein family of basic leucine zipper-type transcription factors, as a target gene of saturated fatty acids/TLR4 signaling in macrophages in obese adipose tissue. Importantly, ATF3, when induced by saturated fatty acids, can transcriptionally repress tumor necrosis factor-α production in macrophages in vitro. Chromatin immunoprecipitation assay revealed that ATF3 is recruited to the region containing the activator protein-1 site of the endogenous tumor necrosis factor-α promoter. Furthermore, transgenic overexpression of ATF3 specifically in macrophages results in the marked attenuation of proinflammatory M1 macrophage activation in the adipose tissue from genetically obese KKA^{y} mice fed high-fat diet. This study provides evidence that ATF3, which is induced in obese adipose tissue, acts as a transcriptional repressor of saturated fatty acids/TLR4 signaling, thereby revealing the negative feedback mechanism that attenuates obesity-induced macrophage activation. Our data also suggest that activation of ATF3 in macrophages offers a novel therapeutic strategy to prevent or treat obesity-induced adipose tissue inflammation. (***Circ Res.* 2009;105:25-32.**)

Key Words: adipocytes ■ ATF3 ■ fatty acids ■ inflammation ■ macrophages ■ TLR4

Known as the metabolic syndrome, the cluster of well-established risk factors for cardiovascular disease (visceral fat obesity, impaired glucose metabolism, atherogenic dyslipidemia, and blood pressure elevation), is an increasing health problem worldwide.[1–3] The pathophysiology underlying the metabolic syndrome is not fully understood and visceral fat obesity appears to be an important component.[4] There is considerable evidence that obesity is a state of chronic low-grade inflammation, which may play a critical role in the pathophysiology of the metabolic syndrome.[1–3]

Obese adipose tissue is markedly infiltrated by macrophages, suggesting that they may participate in the inflammatory pathways that are activated in obese adipose tissue.[5] Using an in vitro coculture system composed of adipocytes and macrophages, we have provided evidence that a paracrine loop involving saturated fatty acids and tumor necrosis factor (TNF)α derived from adipocytes and macrophages, respectively, establishes a vicious cycle that augment the inflammatory change in obese adipose tissue.[6] Recent studies have also pointed to the heterogeneity of macrophages infiltrated into obese adipose tissue, ie, they follow 2 different polarization states: M1, or "classically activated" (proinflammatory) macrophages, which are induced by proinflammatory mediators such as lipopolysaccharide (LPS) and Th1 cytokine interferon-γ; and M2, or "alternatively activated" (antiinflammatory) macrophages, which are generated in vitro by expo-

Original received February 23, 2009; revision received May 11, 2009; accepted May 20, 2009.

From the Department of Molecular Medicine and Metabolism (T.S., X.Y., Y.S., N.N., I.S., Y.K., Y.O.), Department of Biochemical Genetics (S.K.), Global Center of Excellence Program (Y.O.); and International Research Center for Molecular Science in Tooth and Bone Diseases, Laboratory of Recombinant Animals (T.U.), Medical Research Institute, Tokyo Medical and Dental University, Tokyo; Division of Biomedical Research Resources (K.U.-Y., J.M.), National Institute of Biomedical Innovation, Osaka; Kyoto Institute of Nutrition and Pathology (T.T., K.N.); Department of Medicine (Y.M.), Division of Atherosclerosis and Diabetes, National Cardiovascular Center Hospital, Osaka; and Department of Metabolic Disorder (K.Y.), Research Institute, International Medical Center of Japan, Tokyo, Japan.

Correspondence to Yoshihiro Ogawa, Department of Molecular Medicine and Metabolism, Medical Research Institute, Tokyo Medical and Dental University, 1-5-45 Yushima, Bunkyo-ku, Tokyo 113-8510, Japan. E-mail ogawa.mmm@mri.tmd.ac.jp

Circulation Research **is available at http://circres.ahajournals.org** **DOI: 10.1161/CIRCRESAHA.109.196261**

sure to Th2 cytokines such as interleukin (IL)-4 and IL-13.[7–9] Evidence has accumulated indicating that macrophages, which are infiltrated into obese adipose tissue, exhibit the phenotypic change from M2 to M1 polarization.[7–9] Recent evidence also showed that the nuclear receptor peroxisome proliferator-activated receptor-γ or -δ regulates M2 polarization of adipose tissue macrophages and thus systemic insulin sensitivity.[8,9] It is, therefore, conceivable that M1 macrophages induce the release of saturated fatty acids from hypertrophied adipocytes via lipolysis, which, in turn, may serve as a proinflammatory adipocytokine locally in the adipose tissue.

Free fatty acids represent an important energy source mobilized from triglycerides stored in the adipose tissue, particularly during periods of starvation, but recent evidence has suggested the pathophysiologic roles other than the supply of nutrients in times of fasting or increased energy demand.[10] For instance, elevated levels of circulating free fatty acids, which are often associated with visceral fat obesity, increase fat accumulation in insulin target tissues such as the skeletal muscle and liver and contribute to insulin resistance.[11] We and others have reported that saturated fatty acids, which are released from adipocytes via the macrophage-induced lipolysis, serve as a naturally occurring ligand for Toll-like receptor (TLR)4 complex, which is essential for the recognition of LPS, to induce nuclear factor (NF)-κB activation in macrophages.[12–14] Evidence has also suggested that TLR4 plays an important role in adipose tissue inflammation.[14–17] Because macrophages in obese adipose tissue are exposed to saturated fatty acids released in large quantities from hypertrophied adipocytes, there might be negative regulatory mechanisms, whereby macrophages are protected against the saturated fatty acid–induced inflammatory response in obese adipose tissue.

Through a combination of cDNA microarray analyses of saturated fatty acid–stimulated macrophages in vitro and obese adipose tissue in vivo, we identified activating transcription factor (ATF)3, a member of the ATF/cAMP response element-binding protein (CREB) family of basic leucine zipper-type transcription factors[18,19] that is markedly induced in macrophages through TLR4 in response to saturated fatty acids in vitro and in obese adipose tissue in vivo. This study provides evidence that ATF3 acts as a transcriptional repressor of saturated fatty acids/TLR4 signaling in macrophages, thereby revealing the negative feedback mechanism that attenuates obesity-induced macrophage activation in obese adipose tissue. Our data also suggest that activation of ATF3 in macrophages offers a novel therapeutic strategy to prevent or treat obesity-induced inflammation and thus the metabolic syndrome associated with excess adiposity.

Materials and Methods

An expanded Materials and Methods section is available in the Online Data Supplement at http://circres.ahajournals.org.

Materials and Antibodies

Details are provided in the Online Data Supplement.

Animals

Six-week-old male C3H/HeJ mice, which have defective LPS signaling attributable to a missense mutation in the TLR4 gene,[20] and control C3H/HeN mice were purchased from CLEA Japan (Tokyo, Japan). Genetically obese *ob/ob*, *db/db*, and KKA^y mice were purchased from CLEA Japan and Charles River Japan (Tokyo, Japan). Details on experimental conditions are provided in the Online Data Supplement. All animal experiments were conducted in accordance to the guidelines of Tokyo Medical and Dental University Committee on Animal Research (No. 0090058).

Generation of Transgenic Mice Overexpressing ATF3 in Macrophages

Details are provided in the Online Data Supplement.

Cell Culture

RAW264 macrophage cell line (RIKEN BioResource Center, Tsukuba, Japan), 3T3-L1 preadipocytes, and HEK293 (American Type Culture Collection, Manassas, Va) were maintained in DMEM (Nacalai Tesque, Kyoto, Japan) containing 10% FBS (BioWest, Miami, Fla). Differentiation of 3T3-L1 preadipocytes to mature adipocytes was performed as previously described[6,12] and used as differentiated 3T3-L1 adipocytes at days 8 to 10 after the induction of differentiation. Murine peritoneal macrophages and bone marrow–derived macrophages were prepared as described.[12]

Chromatin Immunoprecipitation Assay

Details are provided in the Online Data Supplement.

Retrovirus-Mediated Overexpression and Knockdown of ATF3 in Macrophages

Retrovirus-mediated overexpression of the full-length mouse ATF3 cDNA and knockdown of endogenous ATF3 were performed in RAW264 macrophages as described in the Online Data Supplement.

Quantitative Real-Time PCR

Total RNA was extracted from cultured cells using Sepazol reagent (Nacalai Tesque) and quantitative real-time PCR was performed with an ABI Prism 7000 Sequence Detection System using PCR Master Mix Reagent (Applied Biosystems, Foster City, Calif).[6,12] Primers used in this study are described in Online Table I. Levels of mRNA were normalized to those of 36B4 mRNA.

Histological Analysis

Histological analysis was performed as previously described using the paraffin-embedded sections of the epididymal white adipose tissue.[15] In brief, hematoxylin/eosin staining was used to compare the adipocyte cell size with the software Win Roof (Mitani, Chiba, Japan).[15] The presence of F4/80-positive macrophages in the adipose tissue was detected immunohistochemically using the rat monoclonal antimouse F4/80 antibody[21] as described previously.[15] The number of F4/80-positive cells was counted in more than 10 mm^2 area of each section and expressed as the mean number/mm^2.

Western Blotting of ATF3

Whole cell lysates were prepared as previously described.[6] Samples (20 μg protein per lane) were separated by 12.5% SDS-PAGE and Western blotting was performed using antibodies against ATF3 (Santa Cruz Biotechnology).

Measurement of TNFα Levels in Culture Media

The TNFα levels in culture supernatants were determined by a commercially available ELISA kit (R&D systems, Minneapolis, Minn).[6]

Transient Transfection and Luciferase Assay

Details are provided in the Online Data Supplement.

Statistical Analysis

Data were expressed as the means±SE. Statistical analysis was performed using ANOVA, followed by Scheffe's test unless otherwise described. $P<0.05$ was considered to be statistically significant.

Results and Discussion

Identification of ATF3 As a Target Gene of Saturated Fatty Acids in Macrophages in Obese Adipose Tissue

We have provided in vitro evidence that saturated fatty acids, which are released from adipocytes via the macrophage-induced lipolysis, serves as a naturally occurring ligand that stimulates TLR4 signaling in macrophages.[12] To search for target gene(s) of saturated fatty acids in macrophages in obese adipose tissue, we performed cDNA microarray analysis of obese adipose tissue from *ob/ob* mice and palmitate-stimulated RAW264 macrophages (Online Figure I, a). Upregulated genes under both conditions included chemokines, proinflammatory cytokines, acute phase reactants, and ATF3 (Online Table II), whereas 5 genes were downregulated (Online Table III). ATF3 is a member of the ATF/CREB family of transcription factors.[18,19] ATF3 is rapidly induced in response to several stimuli and insults, such as chemicals, irradiation, and oxidative stress, and, in turn, negatively regulates target genes as a transcriptional repressor.[18,19] Although ATF3 plays a role in apoptosis and cell cycle,[18,19,22] the role of ATF3 in obesity is largely unknown. We, therefore, investigated the tissue distribution of ATF3 in obese and lean mice. Similar to macrophage marker F4/80, ATF3 mRNA expression was markedly increased in the adipose tissue from *db/db* mice relative to wild-type mice (Online Figure I, b). In this study, there was a significant increase in ATF3 mRNA expression in the liver from *db/db* mice relative to wild-type mice ($P<0.01$).

We confirmed our cDNA microarray data by real-time PCR and immunostaining. Expression of ATF3 and F4/80 mRNAs was increased in the adipose tissue during the course of diet-induced obesity (Figure 1A). We also observed upregulation of ATF3 and F4/80 in the adipose tissue from *ob/ob* mice (Figure 1B). Collagenase digestion of the adipose tissue, which is validated by F4/80 and adiponectin mRNA expression, revealed that ATF3 is expressed predominantly in stromal-vascular fraction in the adipose tissue (Figure 1C). Furthermore, ATF3 mRNA expression was increased significantly in *ob/ob* mice fed high-fat diet relative to wild-type mice fed standard diet ($P<0.01$) (Figure 1C). We also confirmed by immunostaining of ATF3 and F4/80 using serial sections of obese adipose tissue that most ATF3-positive cells are stained with F4/80 (Figure 1D). These observations indicate that ATF3 is markedly upregulated in obese adipose tissue, especially in infiltrated macrophages.

Saturated Fatty Acids Induce ATF3 via TLR4 in Macrophages In Vitro and In Vivo

We next examined the involvement of TLR4 in the saturated fatty acid–induced ATF3 mRNA and protein expression in macrophages in vitro. Saturated fatty acids, such as palmitate and stearate, and LPS increased significantly ATF3 mRNA and protein expression in RAW264 macrophages ($P<0.05$ versus vehicle) (Figure 2A through 2D). Interestingly, unsaturated fatty acids, such as oleate and eicosapentaenoic acid, did not affect ATF3 mRNA expression (Figure 2C and 2D and data not shown), suggesting the structure-specific effect of free fatty acids. We found that palmitate fails to increase ATF3 mRNA expression in peritoneal macrophages from C3H/HeJ mice with defective TLR4 signaling (Figure 2E). We also observed that BAY11-7085, an NF-κB inhibitor, markedly inhibits the palmitate-induced ATF3 mRNA expression in RAW264 macrophages (Figure 2F). The data were confirmed using RAW264 macrophages overexpressing a super-repressor form of IκBα (SR-IκBα) (Figure 2G). Furthermore, selective NF-κB activation by transient overexpression of p50 and p65 subunits of NF-κB increased significantly the ATF3 promoter activity in HEK293 cells ($P<0.01$) (Figure 2H). In this setting, the changes in ATF3 mRNA expression were almost parallel to those in TNFα mRNA expression (Figure 2E and 2F and data not shown). These observations indicate that TLR4/NF-κB pathway plays an important role in saturated fatty acid–induced ATF3 and TNFα expression in macrophages. On the other hand, palmitate and stearate, but not unsaturated fatty acids, are known to serve as precursors for de novo ceramide synthesis, thereby inducing inflammatory changes in certain cells.[23,24] However, we observed that pharmacological inhibition of ceramide synthesis slightly inhibits the palmitate-induced ATF3

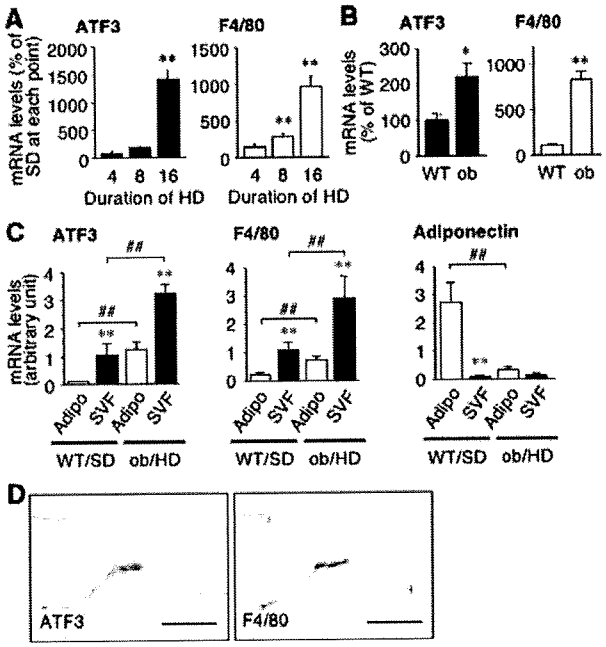

Figure 1. ATF3 expression in obese adipose tissue. ATF3 and F4/80 mRNA expression in the epididymal adipose tissue from high-fat diet (HD)-fed obese mice for up to 16 weeks (A) and genetically obese *ob/ob* mice at 15 weeks of age (ob) (B). *$P<0.05$, **$P<0.01$ vs standard diet (SD) or wild-type mice (WT) (n=6 to 10). C, ATF3, F4/80, and adiponectin mRNA expression in mature adipocytes (Adipo) and stromal-vascular fraction (SVF) in the epididymal adipose tissue from SD-fed WT and HD-fed ob. **$P<0.01$ vs the respective Adipo, ##$P<0.01$ (n=4 to 5). D, ATF3 and F4/80 immunostaining in the epididymal adipose tissue from HD-fed ob. Original magnification, ×400. Scale bars=100 μm.

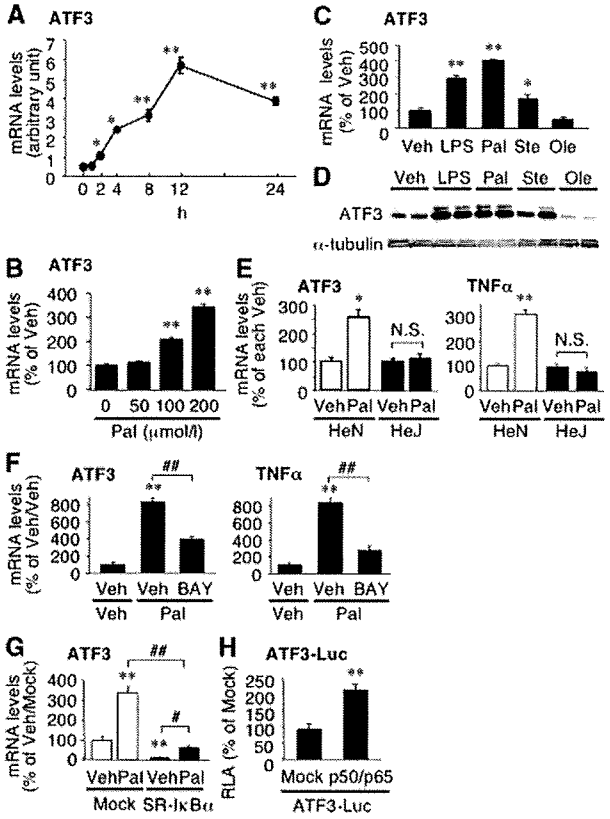

Figure 2. Saturated fatty acid–induced ATF3 expression in cultured macrophages. A, Time course of palmitate-induced ATF3 mRNA expression in RAW264 macrophages. Pal indicates palmitate 200 μmol/L. *$P<0.05$ vs 0 hour. B, Dose-dependent effect of palmitate on ATF3 mRNA expression in RAW264 macrophages. Effect of saturated and unsaturated fatty acids (FAs) on ATF3 mRNA (C) and protein (D) expression in RAW264 macrophages. Veh indicates vehicle; LPS, LPS 10 ng/mL; Pal, palmitate 200 μmol/L; Ste, stearate 200 μmol/L; Ole, oleate 200 μmol/L. *$P<0.05$, **$P<0.01$ vs Veh. E, Role of TLR4 in the palmitate-induced ATF3 and TNFα mRNA expression in peritoneal macrophages. HeN and HeJ indicate peritoneal macrophages from wild-type C3H/HeN and TLR4 mutant C3H/HeJ mice, respectively. *$P<0.05$, **$P<0.01$ vs Veh/HeN. F, Effect of NF-κB inhibitor BAY11-7085 (BAY, 10 μmol/L) on the palmitate-induced ATF3 and TNFα mRNA expression in RAW264 macrophages. **$P<0.01$ vs Veh/Veh, ##$P<0.01$. G, Effect of super-repressor IκBα (SR-IκBα) on the palmitate-induced ATF3 and TNFα mRNA expression in RAW264 macrophages. Mock and SR-IκBα, stably mock-, and SR-IκBα–expressing RAW264 macrophages, respectively. **$P<0.01$ vs Veh/mock; #$P<0.05$, ##$P<0.01$. H, Effect of NF-κB activation on ATF3 promoter activity. The luciferase reporter containing a 1.8-kb human ATF3 promoter fragment (ATF3-Luc) with p50 and p65 subunits of NF-κB or mock was transiently transfected in RAW264 macrophages. **$P<0.01$ vs mock (n=4 to 6).

mRNA expression in RAW264 macrophages (T. Suganami, I. Shirakawa, Y. Ogawa, unpublished data, 2009). These observations, taken together, suggest that saturated fatty acid–induced ATF3 expression is mediated mostly through the TLR4/NF-κB pathway.

We next examined the role of TLR4 in ATF3 expression in the interaction between adipocytes and macrophages. We have established an in vitro coculture system composed of adipocytes and macrophages and found that saturated fatty acids, which are released from adipocytes via the macrophage-induced lipolysis, are capable of activating the TLR4/NF-κB signaling.[6,12] Coculture of 3T3-L1 adipocytes with peritoneal macrophages from C3H/HeN mice resulted in the upregulation of ATF3 and TNFα mRNAs, which was significantly inhibited in the coculture with peritoneal macrophages from C3H/HeJ mice ($P<0.05$) (Online Figure II, a). We found that BAY11-7085 effectively inhibits the upregulation of ATF3 and TNFα mRNA expression in the coculture system (Online Figure II, b).

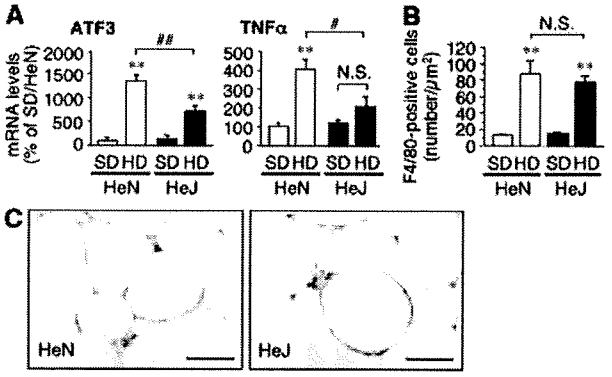

Figure 3. Role of TLR4 in obesity-induced ATF3 mRNA expression in adipose tissue macrophages. ATF3 and TNFα mRNA expression (A) and macrophage infiltration (B) in the adipose tissue from mice fed high-fat diet (HD) or standard diet (SD). **$P<0.01$ vs the respective SD; #$P<0.05$, ##$P<0.01$ (n=6 to 10). C, Immunostaining for ATF3 in the adipose tissue from HD-fed HeN and HeJ. Original magnification, ×400. Scale bars=100 μm.

Using C3H/HeJ and C3H/HeN mice fed high-fat diet, we also examined the involvement of TLR4 in obesity-induced ATF3 expression in the adipose tissue. There were no significant differences in body weight and adipose tissue weight between high-fat diet-fed C3H/HeN and C3H/HeJ mice (Online Table IV). Similar to our previous data on TNFα,[15] the high-fat diet–induced increase in ATF3 mRNA expression was significantly attenuated in the adipose tissue from C3H/HeJ mice relative to C3H/HeN mice ($P<0.01$) (Figure 3A). Importantly, there was no significant change in the number of macrophages infiltrated into the adipose tissue, as assessed by F4/80 immunostaining (Figure 3B), suggesting the attenuation of macrophage activation in C3H/HeJ mice. Immunohistochemical analysis also confirmed the marked reduction of ATF3 staining in C3H/HeJ mice relative to C3H/HeN mice during the high-fat diet (Figure 3C). Collectively, these observations suggest that the saturated fatty acid–induced ATF3 expression in macrophages is mediated via TLR4 in vitro and in vivo.

ATF3 Reduces Saturated Fatty Acid–Induced TNFα Production in Macrophages

To elucidate the functional role of ATF3 in macrophages, we examined the effect of ATF3 overexpression on proinflammatory cytokine production in macrophages in vitro. A full-length mouse ATF3 cDNA was stably overexpressed in RAW264 macrophages by retroviral transduction, which was confirmed by real-time PCR and Western blotting (Figure 4A). In RAW264 macrophages overexpressing ATF3 (ATF3-RAW264), the palmitate- and LPS-induced increase in TNFα